Hybrid Battery Fuel Cell System for Automotive Applications

A Major Qualifying Project
Submitted to the Faculty of
Worcester Polytechnic Institute
In partial fulfilment of the requirements
For the degree in Bachelor of Science
In
Mechanical Engineering
And
Chemical Engineering

By

Lazi Danga

Daniel Dietrich

Tony Eid

Anxhelo Ripa

Tyler Vu

Date: December 20, 2021

Project Advisors:

Professor Robert Daniello (ME)

Professor Andrew Teixeira (CHE)

Professor Ravindra Datta (CHE)

ACKNOWLEDGMENTS

We would like to thank our advisors Professor Daniello, Professor Teixeira, and Professor Datta for their guidance and support throughout the project.

We would also like to thank Doug White from Goddard Hall, Peter Hefti from Higgins Laboratories, Cameron Armstrong, David Kenney, and Patrick Roche for their technical support in the lab.

ABSTRACT

Fuel cells offer an alternative for automotive systems to achieve a performance comparable or better than battery EV and ICEs. We developed a tool that calculates vehicle performance on a track according to design parameters for the fuel cell, drivetrain, and hybrid powertrain to aid a student organized team or similar small-scale vehicle race team in designing a fuel cell powered electric vehicle. Additionally, we determined the polarization curve of an existing fuel cell and demonstrated the impact of cooling on fuel cell performance.

TABLE OF CONTENTS

Page

LIST OF TABLES

Table Page

LIST OF FIGURES

Figure Page

1 INTRODUCTION

Ever since the advent of the industrial revolution, engineers and scientists have found innovative ways to generate power more efficiently. In the case of automotive vehicles, the most common type of system used to provide the required energy is the internal combustion engine (ICE). However, ICEs release greenhouse gases into the atmosphere, which are harmful to the environment. In addition, ICEs use non-renewable energy sources. Furthermore, despite the high-power output of internal combustion engines, their efficiency remains low. As a result, alternative methods have been considered to power automobiles, such as electric battery systems. However, batteries take much longer to recharge (approximately 3-5 hours) than it takes to refuel ICEs (approximately 5 minutes) and they simply shift the use of fossil fuels to earlier in their manufacturing process. In addition to many operational issues, batteries require the use of scarce mineral resources like lithium, which adds cost in the operational and recycling stages. Nevertheless, battery electric vehicles are still quite promising technology that could overtake ICE vehicles if operational and infrastructural obstacles could be addressed.

An alternative to internal combustion and battery powered vehicles is the use of fuel cell systems. Fuel cells capitalize on the chemical energy of the fuel and use the current to power an electric motor of a vehicle. Overall, the vehicle design is like standard battery electric systems except that the rechargeable battery in the battery electric vehicle is replaced with a fuel cell that is pumped from an external station. Fuel cells, like batteries, generate no environmentally harmful emissions. However, fuel cells tend to operate at steady state and offer little reserve if sized to average load.

The hybrid fuel cell-battery system would reduce harmful environmental effects due to the environmental benefits of fuel cell technology while maintaining reliable automotive performance due to the already evolved battery electric infrastructure. Our team set out to design a hybrid fuel cell-battery system for automotive applications. To support the shift to fuel cell vehicles, new design tools will be needed for vehicle manufacturers to optimize the performance of their vehicles. To do so, we used a small student designed race car on campus as a model vehicle to study the integration of hybrid fuel cell-battery technology. Furthermore, we performed experiments on a physical fuel cell to help strengthen our results.

2 LITERATURE REVIEW

This chapter explores relevant technology for hybrid fuel cell-battery systems. We will describe how a fuel cell functions and what components are required for the system, as well as provide a brief historical overview of the technology. Moreover, the automotive applications of fuel cells will be investigated, leading into a discussion of hybrid fuel cell-battery systems. Finally, we will discuss how to experiment on fuel cells, as well as some background on SAE racing, which presents an opportunity to test fuel cell technology.

2.1 Introducing the Fuel Cell

Fuel cells capitalize on the chemical potential energy bound within the molecular structure of a fuel to produce an electric current that can power a wide range of systems, from phones and laptops to automotive vehicles, and even large power plants. Both the fuel cell and battery are classified as a *galvanic cell* (primary power source), a type of electrochemical cell which produces electric current via a spontaneous oxidation reduction (redox) reaction. However, while a battery stores reactant within the cell itself, fuel cells are fed by an external fuel source. A galvanic cell can be contrasted to an electrolytic cell, which utilizes an electric current to undergo a non-spontaneous redox reaction, such as the decomposition of water into hydrogen and oxygen. A rechargeable battery (secondary power source) is a battery which can undergo a spontaneous redox reaction in one direction and a non-spontaneous redox reaction in the other direction. All electrochemical cells consist of two half-cells: the anode and the cathode. Electrons flow out of the anode, which is the positive electrode, whereas the cathode is the negative electrode into which electrons flow.

At the anode of an acid fuel cell, hydrogen is oxidized, releasing electrons and heat, leaving behind a hydrogen cation, which can be expressed by Equation (1).

$$2H_2\ (g) \rightarrow 4H^+(aq) + 4e^- \quad (1)$$

The protons from the above half-reaction are then transported through a semipermeable membrane and arrive at the cathode, the negative electrode, which receives the flow of electrons and protons, thereby reducing oxygen to form water. This process is expressed by Equation (2).

$$O_2\ (g) + 4H^+(aq) + 4e^- \rightarrow 2H_2O \quad (2)$$

By adding Equations (1) and (2), the overall reaction for an acid hydrogen fuel cell can be expressed as such in Equation (3):

$$H_2\ (g) + O_2(q) \rightarrow 2H_2O + Q \quad (3)$$

It should be noted that in a battery, chemical species are reduced at the anode and oxidized at the cathode, whereas in a fuel cell, the opposite occurs. Nonetheless, in both batteries and fuel cells, the anode is the source for an electron current whereas the cathode is a sink for that current (Dicks and Rand, 2018). Figure 1 below is a simplified fuel cell schematic; it depicts the flow of hydrogen fuel and oxygen into the anode and cathode, respectively, as well as the directions of current and water exhaust as a result of the reaction.

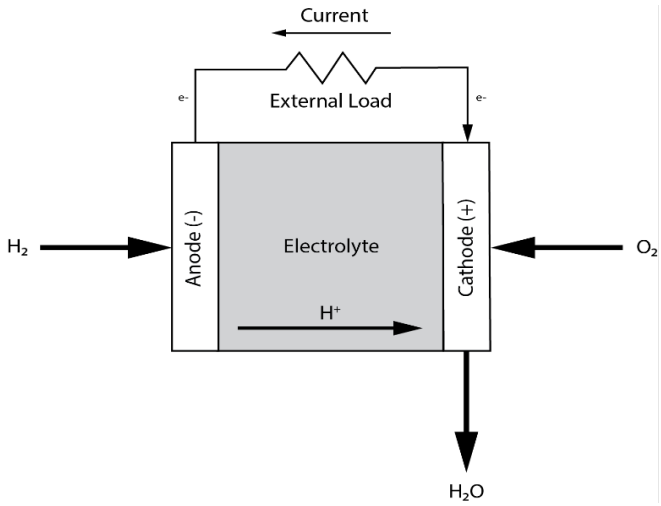

Figure 1: Simplified schematic of a fuel cell showing the flow of hydrogen and oxygen, as well as water exhaust (Bagotsky, 2012).

2.2 Development of Fuel Cell Technology

The electrochemical cell was first discovered by Alessandro Volta at the turn of the nineteenth century when he constructed a Voltaic Pile, the first 'primary' or non-rechargeable power source. The volta disc consisted of a stack of alternating copper and zinc disks that were separated by pasteboard discs soaked in brine. The first fuel cell was properly designed by Sir William Robert Grove in the 1830s to conduct a series of experiments on the newly discovered electrolytic process. Grove called his invention a *gas voltaic battery*, although it is more commonly known as a *Grove cell*, a schematic of which can be seen in Figure 2. The first commercially successful hydrogen-oxygen fuel cell design was done by Ludwig Mond and Carl Langer in 1889, who endeavored to improve the Grove Cell and who were the first to coin the term *fuel cell* for their invention. In 1959, Francis Thomas Bacon patented his first alkaline fuel cell. Bacon's invention spurred greater interest in fuel cell research and development. The Cold War also encouraged innovation in fuel cell technology as the first *proton exchange membrane fuel cells*

(PEMFCs) were used in Project Gemini. However, subsequent NASA expeditions relied on alkaline fuel cells, which were more developed at this time. Other fuel sources were designed and tested, such as *molten carbonate fuel cells* (MCFCs), *solid oxide fuel cells* (SOFCs), and *phosphoric acid fuel cells* (PAFCs). PEMFCs did not become the dominant type of fuel cell technology considered for automotive purposes until the 1990s. At this time, major improvements were made in PEMFC design, such as the introduction of Nafion membranes, improvements in platinum catalyst efficiencies, and improvements in the manufacturing of membrane-electrode assemblies (MEAs) (Bagotsky, 2012; Datta, 2020).

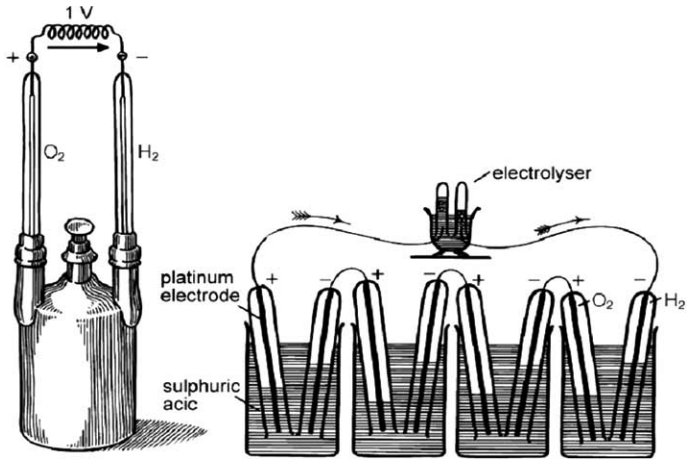

Figure 2: Sketch of Robert Grove's original fuel cell experimental setup (Panayiotou et al.).

2.3 Fuel Cell Components

The primary components of a proton exchange membrane fuel cell are as follows:

- Electrode (Anode)
- Electrolyte Medium
- Electrode (Cathode)
- Fuel Stack (Bipolar Plate)
- Gas Diffusion Layer (GDL)

- Membrane Electrode Assembly (MEA)

An expanded view of these components in a simplified form is shown below in Figure 3.

2.3.1 Electrode (Anode)

On one end of the cell is a negative fuel electrode (anode) that incorporates an electrocatalyst, usually platinum bound to a porous carbon structure for hydrogen-oxygen reactions, which is dispersed on an electronically conducting material. The electrode is fabricated so that the electrocatalyst, the electrolyte, and the fuel come into simultaneous contact at a three-phase boundary (Dicks and Rand, 2018).

2.3.2 Electrolyte Medium

Connected to the anode is the electrolyte medium that conducts ions. Common media include liquid electrolytes such as acids, alkalis, or fused salt, or thin solid polymer or ceramic membranes. The membrane must be an electronic insulator as well as a good ionic conductor and must be stable under both strong oxidizing and strong reducing conditions (Dicks and Rand, 2018).

2.3.3 Electrode (Cathode)

At the other end of the cell is a positive electrode (cathode), also with a triple-point electrocatalyst, on which incoming oxygen is reduced with hydrogen cations by the incoming flow of electrons from the external circuit (Dicks and Rand, 2018).

2.3.4 Fuel Stack (Bipolar Plates)

However, a single fuel cell functions at a low voltage, resulting in most fuel cell applications incorporating a fuel stack to build up the voltage to the desired level by electrically connecting cells in series. These cells are connected by bipolar plates, which electrically connect the cathode of one cell to the anode of the other while also ensuring the flow of hydrogen to the anode and the flow of oxygen to the cathode are separate (Dicks and Rand, 2018).

2.3.5 Gas Diffusion Layer (GDL)

The gas diffusion layer is a permeable membrane that conducts electricity from the catalyst layer to the bipolar plate as well as allowing for the mass transfer of gas from the channels in the bipolar plate to the MEA where the electrochemical reaction takes place (Dicks and Rand, 2018).

2.3.6 Membrane Electrode Assembly (MEA)

The membrane electrode assembly consists of the polymer membrane between two electrocatalyst layers. On the other side of the catalyst layers are the gas diffusion layers (Dicks and Rand, 2018).

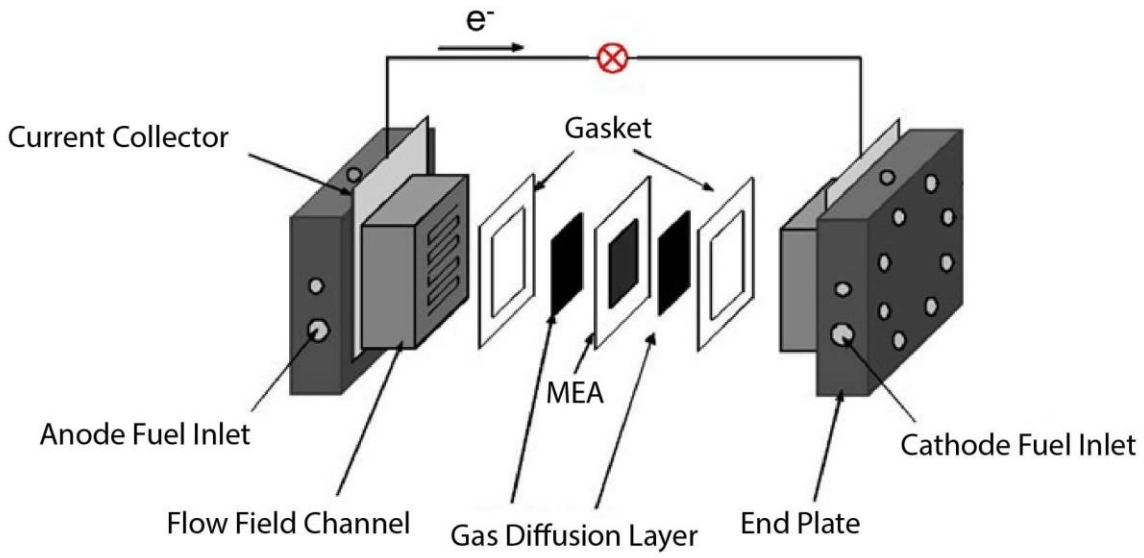

Figure 3: Basic schematic of fuel cell components in an expanded view (Spiegel, 2017).

2.4 Thermodynamic Theory of Fuel Cell Design

The *cell potential*, otherwise known as the *electromotive force* (EMF), or the *reversible open circuit voltage* (OCV), is related to the Gibbs free energy of formation (Δ_fG), which is the maximum reversible energy to do work by a given chemical reaction. The Gibbs free energy of formation is the difference between the energy of formation of the products and reactants as given in Equation (4):

$$\Delta_f G \rightarrow \Delta_f G_{products} - \Delta_f G_{reactants} \tag{4}$$

The *standard equilibrium potential* (the OCV at standard temperature and pressure and at equilibrium) is related to the Gibbs free energy of formation by the following equation:

$$V_0{}^0 = -\frac{\Delta_f G}{nF} \tag{5}$$

Where $\Delta_f G$ is the Gibbs free energy of formation for the overall reaction, n is the number of electrons transferred in the cell by the reaction, and F is the Faraday constant (96845 C mol-1). If the reaction quotient is not equal to the equilibrium value *K*, then the overall cell potential can be written out as:

$$V_0 = V_0^0 - \frac{RT}{nF} \ln Q \tag{6}$$

Where Q is the reaction quotient (the concentration of product species over the concentration of reactant species), R is the gas constant and T is the operating temperature (Datta, 2020; Larminie and Dicks, 2003).

The overall cell potential is not the real output voltage of a cell since it does not account for the efficiencies inherent to the fuel cell. There are potential losses due to kinetic and diffusional processes at both the anode and cathode, ohmic losses, interface resistance, and crossover current. This is represented by the following equation:

$$V = V_0 + (\eta_{+,K} + \eta_{+,D}) + \left(\eta_{-,K} + \eta_{+,D}\right) + i\left(\frac{L_B}{\sigma_B}\right) + i(R_I) \tag{7}$$

These various potential losses grow in magnitude at greater current densities. Thus, a graph of voltage versus current density results in a polarization curve. Figure 4 shows a polarization curve and how large the losses are at the cathode compared to the losses at the anode (Datta, 2020).

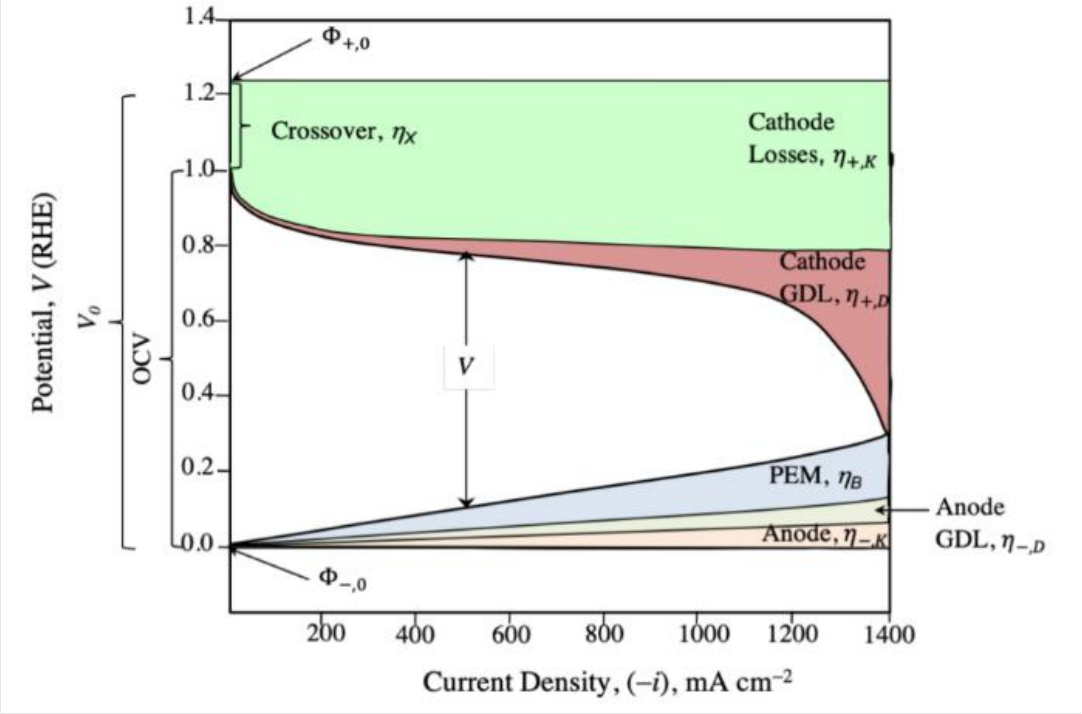

Figure 4: Polarization curve that demonstrates the potential drop of various sources (Datta, 2020).

The shape of the above polarization curve varies by operating pressures and temperatures, partial pressures of hydrogen and oxygen, and even levels of humidity as can be seen in Figure 5 which shows multiple polarization curves for a PEMFC single cell at various conditions.

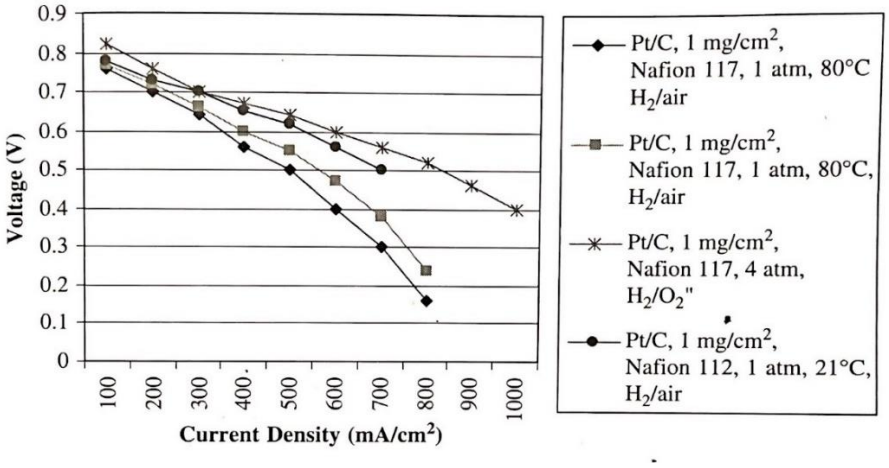

Figure 5: Polarization curve for a PEMFC at variable temperature, pressure conditions, and fuel compositions (Spiegel, 2007).

By relating the cell potential to the Gibbs free energy of formation, the irreversible chemical energy, which is not able to be used for work, is not accounted for. To account for the irreversible chemical energy, the enthalpy of formation (Δ_fH) proves useful. However, there are two different values of Δ_fH that can be used for the reaction of hydrogen with oxygen, depending on whether the latent heat of water (the product of the reaction) is accounted for as liquid of vapor in the products. The higher value of Δ_fH is known as the higher heating value (HHV) whereas the lower value of Δ_fH is known as the lower heating value (LHV). Thus, if all reversible and irreversible chemical energy was transformed into electrical energy, that operating voltage could be calculated by the following equation:

$$V = -\frac{\Delta_f H}{nF} \tag{8}$$

For a hydrogen fuel cell, V_{HHV} = 1.48 V, whereas V_{LHV} = 1.23 V. Thus, the efficiency of a fuel cell is the actual voltage divided by operating voltage.

$$\eta_{HHV} = \frac{V}{1.48V} \quad (9)$$

$$\eta_{LHV} = \frac{V}{1.23\,V} \quad (10)$$

Thus, any efficiency should state whether it is calculated using LHV or HHV, but by convention the LHV is assumed if the actual heating value is not stated when an efficiency is reported (Larminie and Dicks, 2018).

2.5 Fuel Storage

PEMFCs require hydrogen and oxygen as a fuel source. Oxygen can be fed from the atmosphere, whereas hydrogen must be stored within the vehicle. There are numerous methods of storing hydrogen, such as compressed gas, cryogenic liquid, or embedded within carbon nanofibers. Compressed gas is the most practical but is the least energy dense and takes up a large volume. Liquid hydrogen has a greater power density than compressed hydrogen gas, but the double-wall cryogenic tanks and the technology to cryogenically cool hydrogen is expensive. Another method of storying pure hydrogen is by using carbon nanofibers as a scaffold which contains hydrogen molecules in the gaps between the carbon structure (Spiegel, 2007). The issue with carbon nanofiber storage is that it remains at an early stage in research and development. It could prove to be a viable method of hydrogen storage in the future.

Other methods of hydrogen storage involve chemical storage. Metal hydrides have a lower density than both compressed and liquid hydrogen storage. Furthermore, refueling only takes 5-15 minutes. Sodium borohydride can generate hydrogen via hydrolysis and has a high energy density. Other fuel cells do not require direct hydrogen and can instead

use a direct feed of methanol, ethanol, ammonia, sodium borohydride, molten carbonates, and others (Lototskyy, et al. 2017). Due to various complexities, such as the higher costs of cryogenic hydrogen, and concerns about waste management for products associated with chemical storage, we will only consider hydrogen fuel cells in this paper.

2.6 Fuel Cell Applications

Fuel cell technology has been researched and applied in several industries, such as portable power, backup power, stationary power, and transportation. Current applications within the transportation industry include automobiles, buses, utility vehicles and scooters/bicycles (Spiegel, 2007).

The application of fuel cell technology within the automotive industry has gained traction because of increased efforts to make powering vehicles cleaner to the environment. One of the earliest concrete applications of automotive fuel cells was the 1966 General Motors (GM) Electrovan, as seen in Figure 6 below. This was the first fuel cell car ever produced; it was powered by a hydrogen fuel cell with alkaline electrolyte, liquid hydrogen, and liquid oxygen, stored onboard in cryogenic vessels (Helmolt and Eberle, 2007).

Figure 6: 1966 General Motors Electrovan, which shows the fuel cell system with all of its components (Helmolt and Eberle, 2007)

Despite early attempts to introduce fuel cells to the automotive industry on a wide scale, for many years fuel cells were considered to have no substantial advantages over combustion engines nor over batteries, mainly due to the poor power density of the alkaline fuel cells of that time (Helmolt and Eberle, 2007).

Recently, a new hope for hydrogen fuel cell technology have emerged. As mentioned by Jon Hunt, a marketing manager at Toyota, “Every single manufacturer is either looking at or working on hydrogen cars” (Saarinen, 2020). Manufacturers like General Motors, Toyota, and Honda have gone as far as designing their own fuel cells. Companies including Ford, Mazda, Daimler, Hyundai, and Volkswagen have also planned to use fuel cell cars but with the power source designed by contractors like Ballard Systems, DeNora, and UTC fuel cells (Spiegel, 2007). The interesting factor seen for many of these companies is that they started their first demonstrations in the late 1990s or early 2000s. The research behind this technology has been evident although the support from the public was still not present until the 2010s (Speigel, 2007; Saarinen, 2020).

One car that has been produced in recent years is the Toyota Mirai which implements a hybrid approach to cut back on global emissions of carbon dioxide and other pollutants. The Mirai features a fuel cell stack with a maximum output of 128 kW, a nickel-metal hydride battery which can assist the fuel cell or store energy from deceleration, and three fuel tanks that can store a total of 16.8 kg of hydrogen fuel at 70 MPa (700 bar). Along with advances in fuel cell technology and efficiency in the past decade, Toyota was able to address issues concerning cold temperatures start-ups for fuel cell vehicles. Higher fuel cell stack density allows for lower thermal capacity which results in an improved warm-up performance and improved power generating performance (Toyota Mirai Specs & Options, 2021).

2.7 Batteries

Another alternative power source in the automotive industry is the battery electric vehicle, which was led by the need to reduce the emission of greenhouse gases. As of 2017, batteries have been the most expensive component of electric vehicles, accounting for 25 to 50% of the overall cost. Efforts have been made to determine which technology has the highest potential for commercial use (Iclodean, et al., 2017).

In the early 2000s, nickel-metal hydride (Ni-MH) batteries seemed to be the most advanced technology used in hybrid systems. At the time, this technology appeared sufficient as a secondary source of power. In comparison to nickel-cadmium (Ni-Cd) and lead-acid batteries, the Ni-MH fulfilled the power requirements due to its increased energy density and specific energy. Moreover, these batteries allow for regenerative braking and are made of recyclable materials. In comparison, lithium-ion (Li-Ion) batteries, developed

later, offered even more power, as shown in Table 1 below. Li-Ion cells are estimated to increase the specific energy by 20%. However, this energy increase is associated with higher overall system weight, and additional environmental concerns. The general parameters of all battery options are shown below:

Table 1: Comparison of various battery types (Iclodean, et al., 2017).

Name	Value for Battery Type				Unit
	Li-Ion	Na-$NiCl_2$	Ni-MH	Li-S	
Maximum Charge	75	84	85	80	Ah
Nominal Voltage	323	289	288	305	V
Stored Energy	24.2	24.2	24.2	24.2	kWh
Maximum Voltage / Minimum Voltage	339 / 308	275 / 304	274 / 302	290 / 320	V
Initial Charge	100	100	100	100	%
Number of Cells per Cell-Row	12	12	20	26	-
Number of Cell-Row	17	30	20	1	-
Internal Resistance charge/discharge	1 / 1	1 / 1	1 / 1	1 / 1	Ω
Operating Temperature	33	270	36	30	°C
Specific Heat Transition	0.4	6	0.4	0.08	W/K
Specific Heat Capacity	795	950	677	1650	J/kg*K
Mass of Battery	318	457	534	173	kg
Battery Price	300	500	400	250	€

Li-Ion is the most used option for batteries in the EV industry. These batteries lack memory effect, the decrease of the maximum energy capacity in case of repeatedly recharge without being completely discharged. In addition, they offer higher power and specific energy and has the best “charge to weight” ratio. However, Li-Ion batteries also have disadvantages. They have very high operational temperatures which could affect energy performance as well as lifetime and safety (temperature increase cannot be safely used). There are also problems with high production costs, recycling capabilities, and recharging infrastructure as can be seen in Table 1 (Iclodean, et al., 2017). Although Li-Ion is at an advanced research stage, this type of energy source does not satisfy the autonomy requests. The limitations of Li-Ion lead researchers to look for alternative

technologies with higher storage energy capacity (vehicle range) and extended lifespan (Iclodean, et al., 2017).

2.8 Vehicle Energy Source Comparison

The two competing energy sources for electric vehicles (EVs), fuel cells and batteries, may be compared directly with one another. They may also be compared to the internal combustion engine (ICE). The following list highlights the primary points of comparison between these competing automotive energy sources:

1. Costs: Although fuel cell EVs (FCEVs) have higher capital and operating costs than battery EVs (BEVs), FCEVs have the potential to become the cheaper alternatives
2. Range and Refueling: FCEVs have a longer driving range associated with much shorter refueling times than BEVs.
3. Infrastructure requirements: hydrogen stations can serve more vehicles than EV chargers due to the lower refueling times.
4. Lifetime: batteries are affected by climate, overcharging, deep discharge and high charging/discharging rates. Tesla expects batteries to survive for 10 to 15 years but these vehicles are currently untested. In contrast, hydrogen systems can undergo fast refilling, frequent deep discharging without compromising lifetime. “Fuel cell stacks are expected to outlive other drivetrain components” (Staffell, et.al, 2018)
5. User Experience: FCEVs offer a smoother driving experience than ICEs.
6. Emissions: Fuel Cell systems have zero emissions when in use and have a low-carbon production. In addition to FCEV, battery systems also have zero emission

during use. Current, ICE can be improved based on the fuel being used but cannot lower their emissions to zero.

2.9 Electric Motors

In addition to selecting an energy source, the powertrain consists of an electric motor. When it comes to selecting a type of motor for motion generation applications, there are multiple factors that need to be considered. Different motors will have various advantages and disadvantages when compared with one another. There are two main types of motors: Direct Current (DC) and Analog Current (AC) motors. DC motors are either brushless or brushed. A brushless DC (BLDC) motor is similar in construction to an AC motor, but controller implementation is the core difference between each type; in a BLDC motor, electric controllers feed full positive and negative current to two phases at a time, which is ideal for logic controllers and battery power sources that operate on DC. This makes BLDC motors popular in applications such as computers and cars. On the other hand, an AC motor relies on a sinusoidal current supplied to each of its two legs with the appropriate phase difference (Gambhir and Jha, 2013).

Like all other motors, a BLDC motor has a rotor and stator. Windings in a BLDC motor stator are arranged in one of two patterns: a star pattern or a delta pattern. The star pattern gives a high torque at low rotational velocity, while the delta pattern gives low torque at low rotational velocity. The reason for this is that the delta configuration applies half of the voltage across the winding that is not driven, which increases losses, efficiency, and torque. BLDC motors have either a slotted or slot-less core. The slot-less core is usually preferred since it can run at very high speeds due to the lower inductance in comparison to

slotted cores. The main disadvantage of a slot-less core is higher cost compared to slotted cores (Gambhir and Jha, 2013).

Unlike a brushed DC motor, a BLDC motor is controlled electronically using logic; to rotate the BLDC motor, the stator windings are energized in sequence. BLDC motors have several advantages over brushed DC motors. To begin with, BLDC motors do not require maintenance while brushed DC motors do, since the carbon brushes within brushed DC motors wear out quickly after use. Moreover, BLDC motors generate less noise, and are typically smaller and lighter than brushed DC motors. Lastly, and perhaps most importantly, BLDC motors are cleaner, more powerful, have higher speed ranges and dynamic responses, than brushed DC motors, while outlasting brushed DC motors in total operating hours. While running a BLDC motor outside of its specs shortens its lifespan, the typical BLDC motor can last over 20,000 operating hours (Gambhir and Jha, 2013).

When selecting a BLDC motor for a given application (such as the output of a fuel cell system), one must first understand the requirements of the application; this entails understanding the required toque, speed, size, power, and so on, for the given system. Moreover, the controller must also be considered this this component will control the logic of the motor (Gambhir and Jha, 2013).

2.10 Hybrid Battery Fuel Cell Systems

Due to the challenges of utilizing fuel cells in electric vehicles, the adoption rate of the technology in vehicle applications has been very limited. As of 2019, approximately 13,000 fuel cell vehicles are in operation worldwide. The primary issues are related to cost, durability, and user experience, and the infancy of the hydrogen market in regards to

production, distribution, and storage of hydrogen based fuel (Spiegel, 2007; Ma et al., 2020).

The high cost is due to expensive precious metals like platinum in the catalytic layer. On the infrastructure side, the purification process and the supporting refueling stations for hydrogen cannot support the widespread commercialization of fuel cell vehicles. Durability of fuel cell vehicles are not at the level of internal combustion engines which last an average 20,000 hours compared to 8,000 hours. One of the most significant contributors to low market acceptance is the issue of cold starts. Starting a fuel cell stack below 0 °C causes damage to the membrane electrode assembly thus reducing conductivity. Reduced voltage as well as icing around sensitive electronics causes a significant reduction in on-demand power that drivers typically use to in other vehicle types. To reduce these shortcomings, an innovative solution is combining fuel cells with batteries in a hybrid power distribution system (Ma et al., 2020).

2.10.1 Benefits of Hybrid Systems

The addition of an auxiliary power supply from a battery is beneficial for the market acceptance of fuel cell vehicles. Many of the issues associated with fuel cells can be offset by the addition of a technology that already well established. A hybrid combination of batteries with fuel cells is one option. Fuel cells are a relatively new technology which do not have a large enough operation to offset costs, whereas batteries have been in production for a longer span of time which has allowed for the development of supporting infrastructure and lower costs. Adding a battery to a fuel cell as a hybrid system can help bridge the gap of making fuel cells a mainstream technology (Ma et al., 2020).

The user experience of fuel cell vehicles is greatly improved by hybridization with a battery. The three main scenarios that hybridization improves is maximum power output, regenerative braking, and power fluctuations. During high acceleration, the battery can be used as the primary or majority source which allows for instantaneous power. During deceleration and braking, the motor can act like a generator to recharge the battery while the motor is spinning (and not being driven). Additionally, power fluctuations in the fuel cell stack due to non-consistent driving situations can be alleviated. This also extends the lifespan of the stack which can degrade during power fluctuations (Ma et al., 2020).

2.10.2 Components and Controls of Hybrid Systems

The most widely accepted hybrid configuration for fuel cell battery system is the series-parallel hybrid (shown in Figure 7). In this method, the fuel cell and battery are not connected to a separate motor. Additionally, the fuel cell is connected in series with the battery to the motor and the batter is in parallel with the motor. This represents the fundamental scheme required and does not include other components such as controllers and thermal management (Ma et al., 2020).

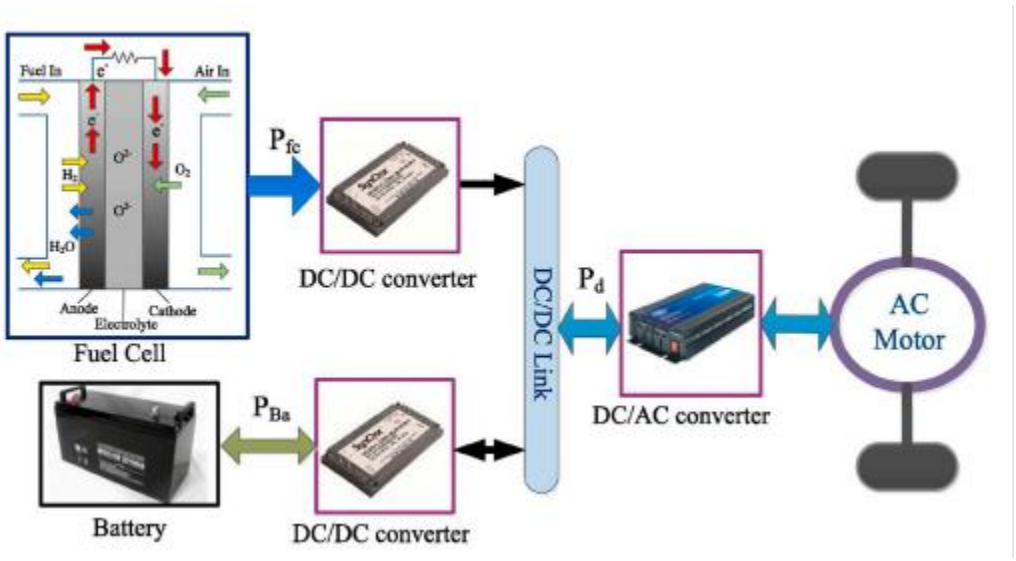

Figure 7: Basic schematic of hybrid battery fuel cell vehicle (Ma et. al., 2020).

Under this system hybridization has three power flow scenarios. During high acceleration the battery and fuel cell work together to handle peak power (Figure 8: Scenario 1). During regenerative braking, energy generated from the motor is put back into the battery (Figure 8: Scenario 2). During cruising conditions, the fuel cell powers the motor and charges the battery at the same time (Figure 8: Scenario 3) (Ma et al., 2020).

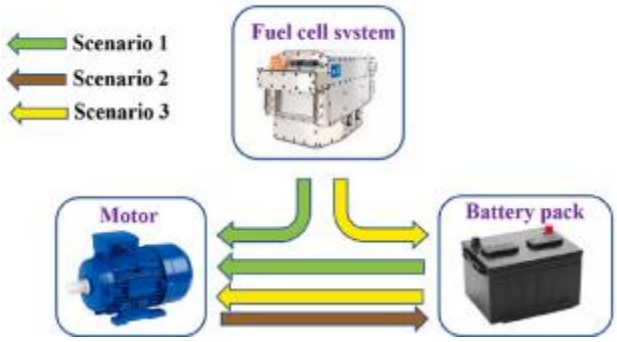

Figure 8: Power flow diagram for hybrid power distribution between fuel cell system, battery pack, and electric motor (Ma et al., 2020).

The model (as shown in Figure 7) contains a fuel cell, battery, and multiple voltage converters. The fuel cell provides the main power source while the battery is used as an auxiliary source. Both sources pass through a DC/DC converter to match the voltages and the battery can recapture energy from braking and from the fuel cell. Finally, the DC/AC converter converts the direct current from the power sources to alternating current for the AC motor (He et al., 2021).

2.11 Experimenting on Fuel Cell Systems

To enhance the study of hybrid fuel cell-battery systems, experimental tests may be conducted. The two model types are active and passive hybrids. Active systems have a DC/DC converter between the battery and fuel cell while passive systems have a single converter in line with one of the two sources. The benefit of the active system is that power sharing between sources can easily be controlled while the passive system benefits from being a less complicated configuration. The system shown in Fig. 8 for vehicles is an active hybrid model. Figure 9 below shows the schematic for a passive model. (Chen et al., 2013)

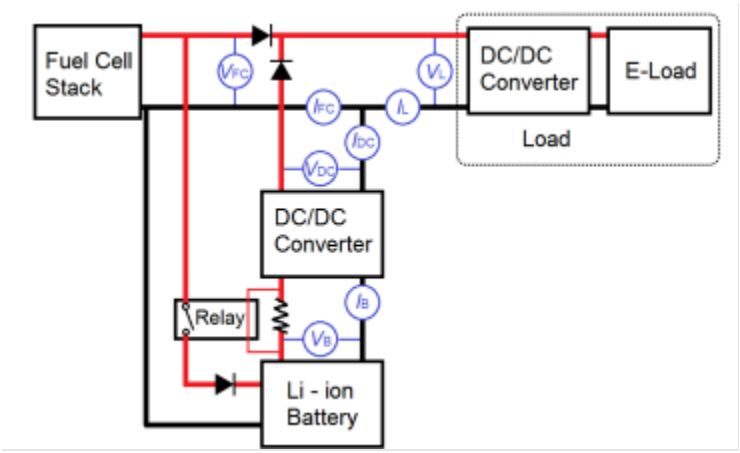

Figure 9: Passive hybrid fuel cell battery system (Chen et al., 2013).

Fuel cells may also be utilized as a sole, independent power source. This may be accomplished by connecting a fuel cell system to an appropriate power source. The fuel cell will then need to be connected directly to an electric load that will accept the current generated by the fuel cell and function as a motor. Additionally, a source of hydrogen will need to feed into the fuel cell system in a manner that allows for the control of the inlet hydrogen pressure. This is achievable by using a pressure regulator on a hydrogen tank. In order to draw results from a functioning fuel cell, a controller may be used to display data, or an electric load may be used that displays results itself. There are electrical loads that can operate in three modes: constant current, constant voltage, or constant power. The constant current function is most applicable for fuel cell tests, since setting the current to a specific value mimics the behavior of changing motor speeds. Once the fuel cell generates the required current, the electrical load outputs values for either voltage or power, or both.

Using an electrical load with the constant current mode with a fuel cell can be useful in multiple ways. For instance, a polarization curve may be created for a fuel cell by incrementally increasing the current on the electrical load and noting the voltage for each corresponding current. Multiple polarization curves may also be created by varying the inlet pressure of the hydrogen; this would be useful in determining how varying the inlet pressure of the hydrogen impacts the performance of the fuel cell system by comparing the various polarization curves. Moreover, temperature experiments may be conducted to better understand the rate of heat loss of a fuel cell, which would be useful for designing a thermal management system.

2.12 The SAE Race Car: A Hybrid Fuel Cell Design Study

A power system must be designed with a set of parameters and requirements, that will provide us with the necessary tools to integrate our hybrid design into an automotive application. One way to obtain parameters and requirements may be from the Society of Automotive Engineers for convenience. The Society of Automotive Engineers (SAE) designs and fabricates a small formula vehicle to compete in the Formula SAE competitions. Both internal combustion engine vehicles (ICE) and electric vehicles (EV) compete in Formula SAE competitions. However, the focus of this project will primarily consider the electric vehicle specifications. These competitions have strict rules and guidelines that need to be followed for a vehicle to compete in the race. For the purposes of this project, rules and regulations for car size, battery output, fuel storage, and safety requirements are considered and used as a baseline for the application of a fuel cell in the Formula SAE car (Formula SAE Rules, 2021). Note that we are not designing a vehicle for competition (pure battery) but rather we are using the formula SAE car as a model system to generate requirements for this design study.

2.12.1 Limitations and Rules

The SAE car rules are designed for the safety and fairness of all students participating in the design and fabrication of the vehicle, therefore certain limitations are necessary. The vehicle must have a minimum wheelbase of 1525mm, and the entire fuel system must be within the primary structure. For electric vehicles, an accumulator container, in which all the battery cells or super capacitors that store the electrical energy to be used by the Tractive System, must be a part of the car and must house the battery

which powers the drivetrain. The container must be constructed of aluminum and is intended to withstand the following accelerations: 40 g in the longitudinal direction, 40 g in the lateral direction, and 20 g in the vertical direction (Formula SAE Rules, 2021).

Electrical limitations for the SAE electric cars include a cap on voltage storage and power drawn and energy meter requirements. The electric vehicle may not draw more than 80kW from the accumulator and the maximum voltage between two points in the vehicle at any time cannot exceed 600 Volts DC. In addition, regenerative energy may be used so long as the speed is greater than 5 km/hr. An energy meter must be present on all SAE vehicles. This ensures that all power generated in the vehicle is accounted for can be checked easily (Formula SAE Rules, 2021).

Fuel tank limitations are applicable to this project since storage of the hydrogen fuel will be necessary. Although the fuel for the SAE car will not be using hydrogen, the safety requirements will still be valid for any combustible fuel. It is important that the fuel tank is made of a rigid substance or contained within a rigid substance to prevent leakage or deformation of the tank. The tank should also be properly secured to the vehicle with some allowed flexibility as to not put unnecessary load on the tank. Any fuel tank size may be used so long as it does not have a variable capacity and it can be emptied if necessary (Formula SAE Rules, 2021).

3 METHODOLOGY

3.1 Objectives

Our goal was to build a design tool that an SAE team or similar small scale vehicle race team could use to design a fuel cell powered electric vehicle. The tool would calculate the vehicle's performance on a track according to design parameters for the fuel cell, drivetrain, and hybrid powertrain. To achieve this the following objectives were outlined:

1. Devise a track as a control variable to test kinematic demands of vehicle performance and determine calculations to map the performance.
2. Develop a preliminary fuel cell design to meet power requirements for racecars according to SAE rules.
3. Design a hybrid fuel cell-battery system to optimize fuel cell performance.
4. Package objectives 1-4 in MATLAB as a tool that could be run to calculate the effects of changes in fuel cell design, battery hybridization, electric motor, vehicle specifications, and track dimensions.
5. Perform experimental test on an existing fuel cell to confirm concepts from our design and learn more about the heat management of the fuel cell.

3.2 Overall Track Specifications

The racetrack used in this experiment is a basic oval-shaped course found in most Indy-car and NASCAR races. The track was assumed to have no incline or banks on any of the turns for simplicity. This allowed for assumptions of only vertical forces acting on the vehicle on the straight sections and centripetal forces included on the sections of track where the vehicle makes a turn. The specific dimensions of the track were determined by

the car requirements which were based on SAE rules and specifications. The radius of each turn was 12 meters, and each straightaway section is 250 meters in length.

The track was broken into eight sections, but all sections had a symmetrical corresponding section on the opposite side of the track as seen below in Figure 10. The straight sections labeled 1, 2, and 3 were designed such that the vehicle could achieve maximum speed and a brief period where it could cruise before decelerating into the turn section. Each of these track sections will be discussed in further detail in the next sections.

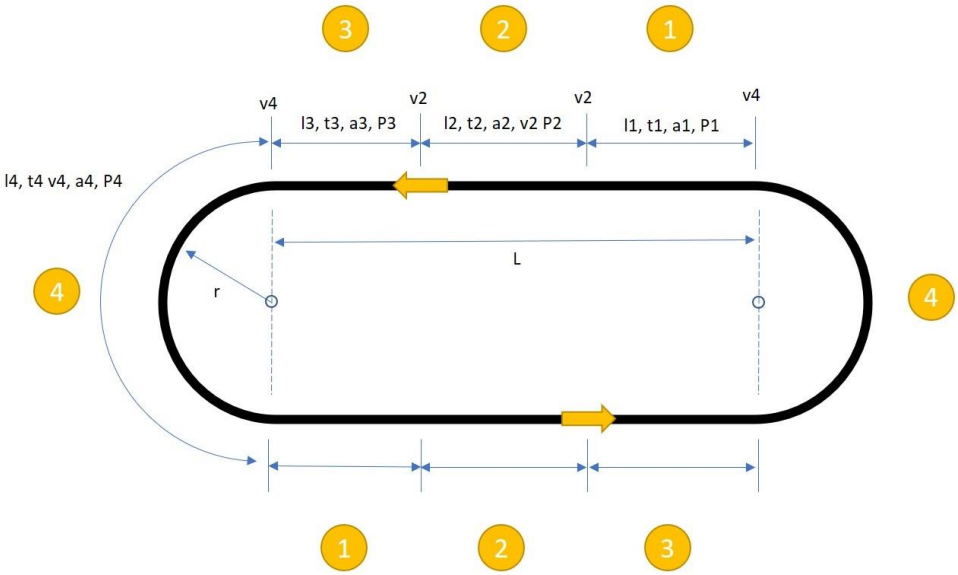

Figure 10: Theoretical racetrack for modelling purposes (not drawn to scale).

3.3 Kinematic Design

The kinematic model that we developed in MATLAB describes each section of the track by a defined function. Each function outputs several variables that are necessary to our design, such as maximum acceleration, maximum velocity, track length, and the time

duration to complete each section. In addition to these variables, the model outputs the power requirements at any single moment of time on the track.

The main inputs for the model are general specifications of the vehicle, the size of the track, motor specifications, fuel cell design specifications, and hybrid parameters. The final output of the kinematic model shows maximum performance at each segment as well as the corresponding plots. The output also shows the fastest possible lap time. The individual parts of the model (track specs and calculations for performance at each section) are described in the following sections.

3.3.1 Modelling the Turns of the Course

An expression for the maximum velocity of the car around the turn was found by drawing out the forces acting on the vehicle around the turn. Assuming the car maintains this maximum velocity around the turn and that the road does not bank, the forces acting on the car may be displayed in the following free body diagram (in Figure 11):

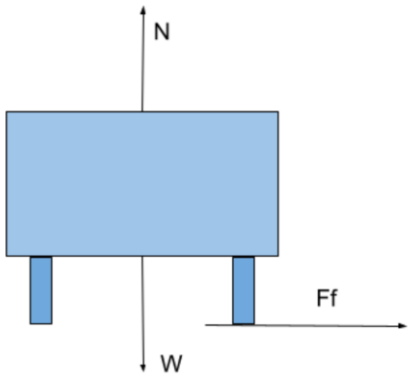

Figure 11: Free body diagram of a vehicle in turn.

The only force acting in the radial direction is the force of friction. This keeps the car from slipping off the road. We may set this friction force equal to the mass of the vehicle multiplied by the centripetal acceleration, since the vehicle is in a turn:

$$\Sigma F_x = F_f = ma_c \tag{12}$$

Where m is the mass of the vehicle and a_c is the centripetal acceleration. Next, the forces in the vertical direction may be expressed, neglecting aerodynamic downforce:

$$\Sigma F_y = N - mg = 0 \rightarrow N = mg \tag{13}$$

Where N is the normal force of the ground acting on the vehicle and g is the acceleration due to gravity. Next, the force of friction is known to be equal to the product of the normal force and the coefficient of friction. Thus, the force of friction may be written as the product of mass, the acceleration due to gravity, and the coefficient of friction:

$$F_f = mg\mu \tag{14}$$

Where μ is the static coefficient of friction between the tires and the ground. Moreover, the centripetal acceleration may be written in terms of the linear velocity of the vehicle and the radius of the turn:

$$a_c = \frac{{v_0}^2}{r} \tag{15}$$

Where v_0 is the maximum linear velocity of the vehicle around the turn, and r is the radius of the turn. These terms for friction and centripetal acceleration may now be substituted into the expression modelling the forces in the horizontal direction, and the linear velocity may be solved for:

$$F_f = ma_c \rightarrow mg\mu = m\frac{{v_0}^2}{r} \tag{16}$$

$$\therefore v_0 = \sqrt{\mu g \mathrm{r}} \tag{17}$$

Therefore, with the coefficient of friction and the acceleration due to gravity being constants, the maximum forward velocity of the vehicle is dependent only on the radius of the turn which is selected in the design of the track. The calculations for this were assumed for vehicles with low center of gravity such as the SAE vehicle.

This expression for the maximum velocity of the vehicle around each turn may now be used to find the minimum power output of the hybrid system needed to overcome the losses for each of the two turns. This equation is shown below:

$$P_{output,1} = \frac{mav_0 + mgv_0 C_{RR} + \frac{1}{2}\rho C A {v_0}^3}{\eta_{drivetrain}} \tag{18}$$

Where a is the linear acceleration of the vehicle, C_{RR} is the rolling resistance between the tires and the ground, ρ is the density of air, C is the drag coefficient due to air resistance, A is the frontal area of the vehicle, and $\eta_{drivetrain}$ is an efficiency value that accounts for minimal additional losses in the vehicle. C_{RR} can range depending on specific tire compound, tread, pressure, as well as operating conditions (Vielstich, 2003). This typically ranges from 0.01 to 0.03. In the model, it is assumed that the vehicle runs at the maximum allowed turning velocity before slipping from the start to the end of each turn. Thus, for each of the two turns, the forward acceleration of the car is zero. Therefore, this power expression simplifies to:

$$P_{output,1} = \frac{mgv_0 C_{RR} + \frac{1}{2}\rho C A {v_0}^3}{\eta_{drivetrain}} \tag{19}$$

3.3.2 Modelling the Straight-Line Acceleration Section

As the turn ends, the vehicle will begin to accelerate and eventually reach a maximum linear velocity, at which it cannot accelerate any further. The acceleration model was assumed to be linear; the car jumps up to its maximum acceleration at the start, after which the acceleration will decrease linearly until it hits zero, where maximum velocity is obtained. It is important, therefore, to know what the maximum theoretical acceleration of the vehicle is. This can be calculated by multiplying the static coefficient of friction between the tires and the road:

$$a_{max} = \mu g \tag{20}$$

With the maximum acceleration, an equation for the linearly varying acceleration may be written. A linear model for acceleration was selected due to the relative simplicity of a linear model, while still serving as a reasonable representation of vehicle acceleration. The maximum acceleration will be the intercept of the dependent variable axis, while the slope, a negative value, will be an arbitrary value that the user can input depending on their application. The independent variable, in this case, is time. Thus, the acceleration expression may be written as follows:

$$a(t) = a_{max} - jt \tag{21}$$

Where j is the rate at which the linear acceleration decreases (acceleration jerk), and t is time as the independent variable. This expression is shown in Figure 12 which uses an arbitrary acceleration jerk. Ideally, the value for jerk is an input that is determined from throttle mapping. Note that the forward acceleration model concludes once it reaches zero, as the maximum forward velocity will be achieved at this time:

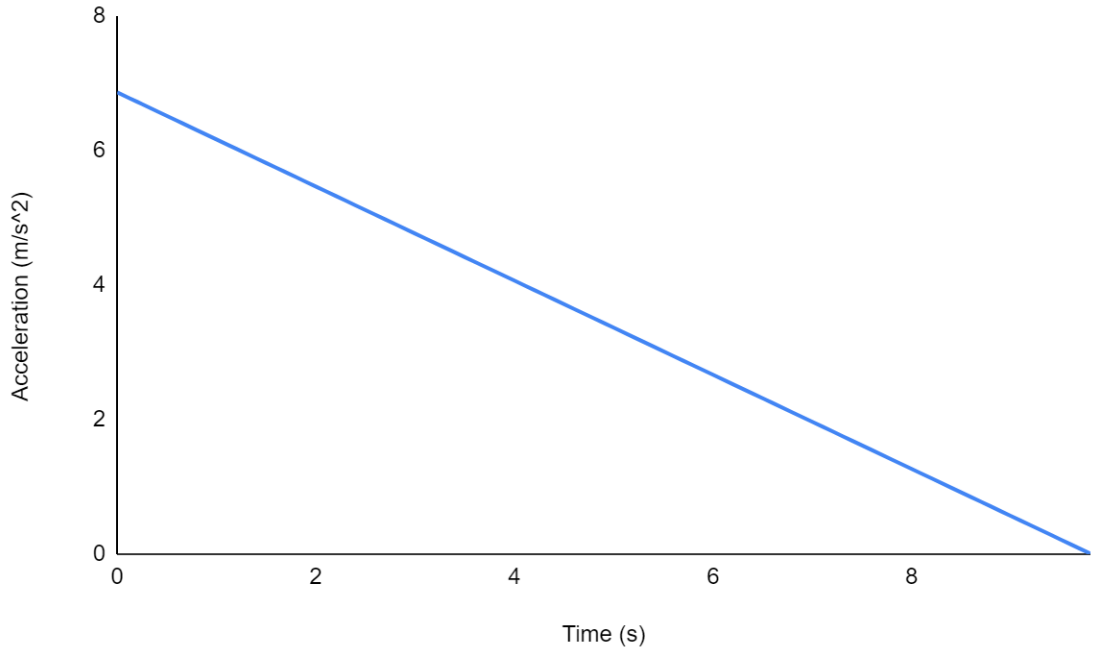

Figure 12: Plot of forward acceleration over time for equation derivation purposes.

Knowing that velocity is the integral of acceleration, the velocity model of the car for this part of the track may be found:

$$v(t) = \int a(t)\,dt \rightarrow v(t) = \int (a_{max} - jt)\,dt \tag{22}$$

$$v(t) = a_{max}t - \frac{jt^2}{2} + v_0 \tag{23}$$

Where v_0 is the initial velocity of the vehicle at the start of this section of the track, which is equal to the velocity of the vehicle during the turn, from the previous section of the track. This velocity expression is shown in Figure 13, using the same acceleration jerk value as the acceleration plot:

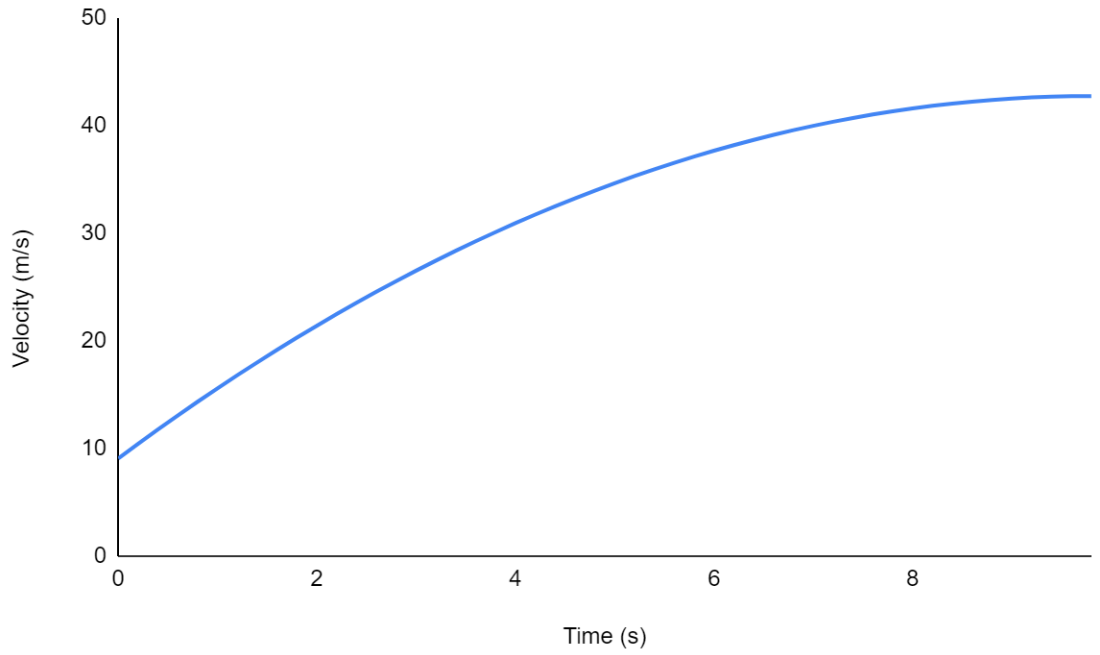

Figure 13: Plot of forward velocity over time for equation derivation purposes.

Now, with these expressions for velocity and acceleration, an equation for the total required power of the vehicle for this section of the track may be written:

$$P_{output,2} = \frac{ma(t)v(t) + mgv(t)C_{RR} + \frac{1}{2}\rho CAv(t)^3}{\eta_{drivetrain}} \tag{24}$$

This required power expression for the acceleration section of the track edges us closer towards understanding the total required power of the vehicle along the entire track, for one full lap.

A further step we may take in this model is finding an expression for the position of the vehicle along the straight-line acceleration section of the track. This can be accomplished by integrating the velocity expression, as shown in the following:

$$x(t) = \int v(t)\,dt \rightarrow x(t) = \int \left(a_{max}t - \frac{jt^2}{2} + v_0\right) dt \tag{25}$$

$$x(t) = a_{max}t^2 - \frac{jt^3}{6} + v_0 t \tag{26}$$

This expression for position over time on the track section for which the vehicle accelerates is represented in Figure 14 below:

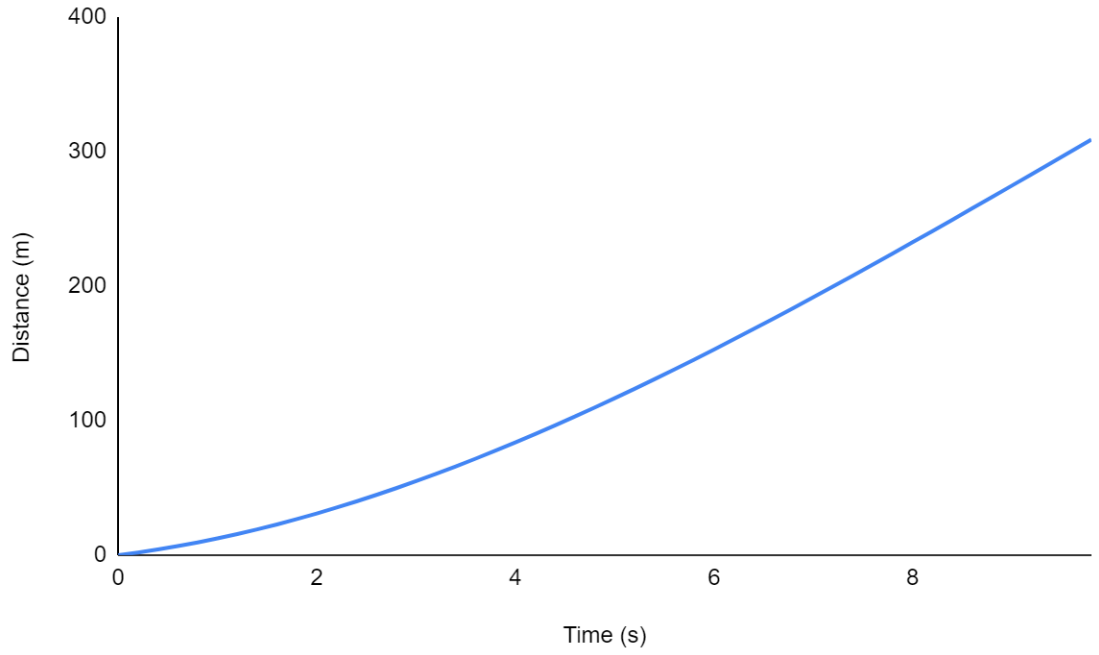

Figure 14: Plot of distance over time for equation derivation purposes.

3.3.3 Modelling the Straight-Line Constant Velocity Section

In our simulation, as the vehicle accelerates in a straight-line, it eventually reaches its maximum velocity. There is a section in our track model in which the vehicle maintains this constant maximum acceleration, before it begins to decelerate, in preparation for the next turn. Thus, a required power expression will need to be written for this constant velocity section of the track (Vielstich, W. et al, 2003). With no acceleration and a constant

velocity, the minimum output expression needed to overcome the losses for this section of the track would be the following:

$$P_{output,3} = \frac{mgvC_{RR} + \frac{1}{2}\rho CAv^3}{\eta_{drivetrain}} \quad (27)$$

The length of the track taken by the car driving at this straight-line constant velocity may also be found. This can be done by subtracting the length of track taken by the acceleration and deceleration phases from the total length of the straight-line section of the track, which we have set to 250 m:

$$l_2 = L - (l_1 + l_2) \quad (28)$$

Where l_2 is the length of the straight-line constant velocity section of the track, L is the total length of the straight-line section, $l_1$is the length of the acceleration straight-line section, and l_3 is the length of the deceleration straight-line section. While the length of the acceleration straight-line section may be found using the distance covered over time expression deduced in the previous section, the length of the deceleration straight-line section will be covered in the next section.

3.3.4 Modelling the Straight-Line Deceleration Section

After the vehicle travels for a certain distance on the straight-line section of the track at the maximum velocity, it will decelerate and enter the next turn of the track at the maximum turning velocity, which was determined in Section 3.3.2. In our model, the car will decelerate at a linear rate, just like the acceleration section. Going into the deceleration section, the vehicle is at maximum velocity (no acceleration), so the deceleration model for this section should start at 0. The deceleration will linearly drop until it reaches a

maximum deceleration value. This maximum deceleration will occur at the instant right before the vehicle reaches the maximum turning velocity, calculated in section 2.3.1. The rate at which the deceleration changes, the deceleration jerk, will also be an arbitrary value that the user may set depending on the application. Thus, the deceleration equation may be written as:

$$a(t)_2 = -j_2 t \tag{29}$$

Where j_2 is the deceleration jerk, while t is once again the time as the independent variable. Figure 15 is a graphical representation of this deceleration expression:

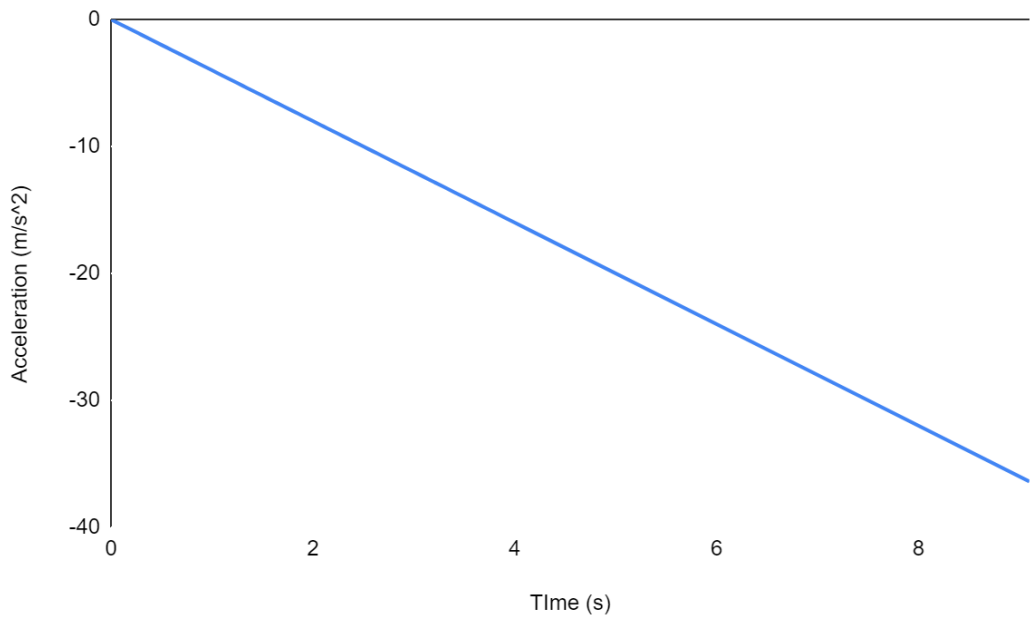

Figure 15: Plot of acceleration over time for equation derivation of deceleration.

Once again, the varying velocity for the deceleration section may be found by integrating the deceleration expression:

$$v(t)_2 = \int a(t)_2 \, dt \rightarrow v(t)_2 = \int (-j_2 t) \, dt \tag{30}$$

$$v(t)_2 = -\frac{j_2 t^2}{2} + v_{max} \tag{31}$$

Where v_{max} is the maximum forward velocity of the vehicle, which is the initial velocity of this deceleration section. Figure 16 is a graph of this velocity over time for the deceleration section:

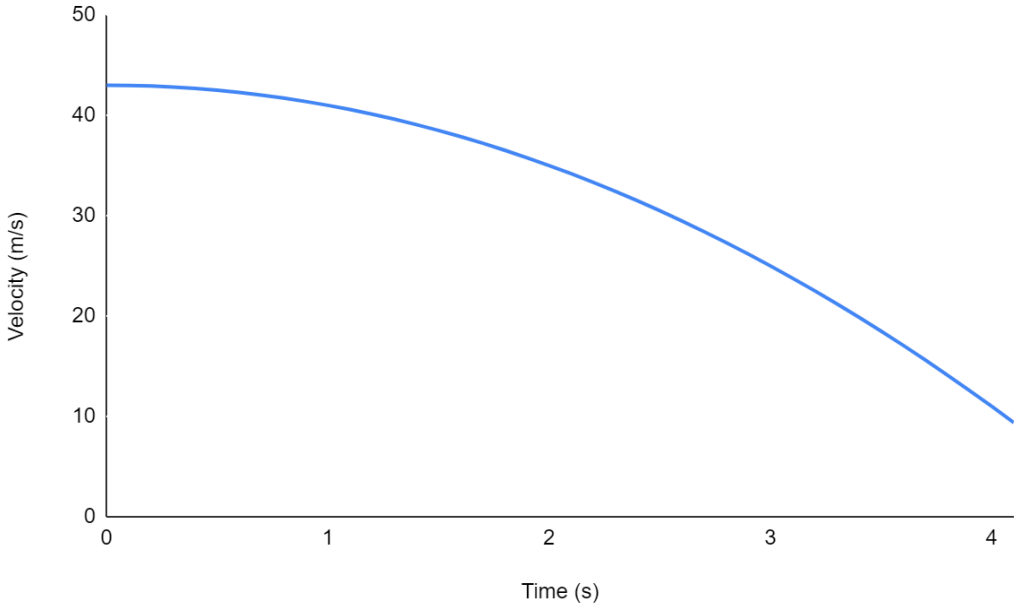

Figure 16: Plot of velocity over time for equation derivation of deceleration.

With the expressions for deceleration and velocity, the minimum power output of the hybrid system needed to overcome the losses may now be modeled for the straight-line deceleration section of the trac. The power expression for this section of the track may be simplified to exclude the mav expression, since the vehicle is not accelerating for this timeframe:

$$P_{output,4} = \frac{mgv(t)_2 C_{RR} + \frac{1}{2}\rho C A v(t)_2{}^3}{\eta_{drivetrain}} \tag{32}$$

Next, we may find an expression for the position of the vehicle along the straight-line deceleration section of the track. This can be accomplished by once more integrating the velocity expression, as shown in the following:

$$x(t)_2 = \int v(t)_2 \, dt \rightarrow x(t)_2 = \int \left(-\frac{j_2 t^2}{2} + v_{max}\right) dt \tag{33}$$

$$x(t)_2 = -\frac{jt^3}{6} + v_{max}\, t \tag{34}$$

This expression for position over time on the track section for which the vehicle accelerates is represented in Figure 17 below:

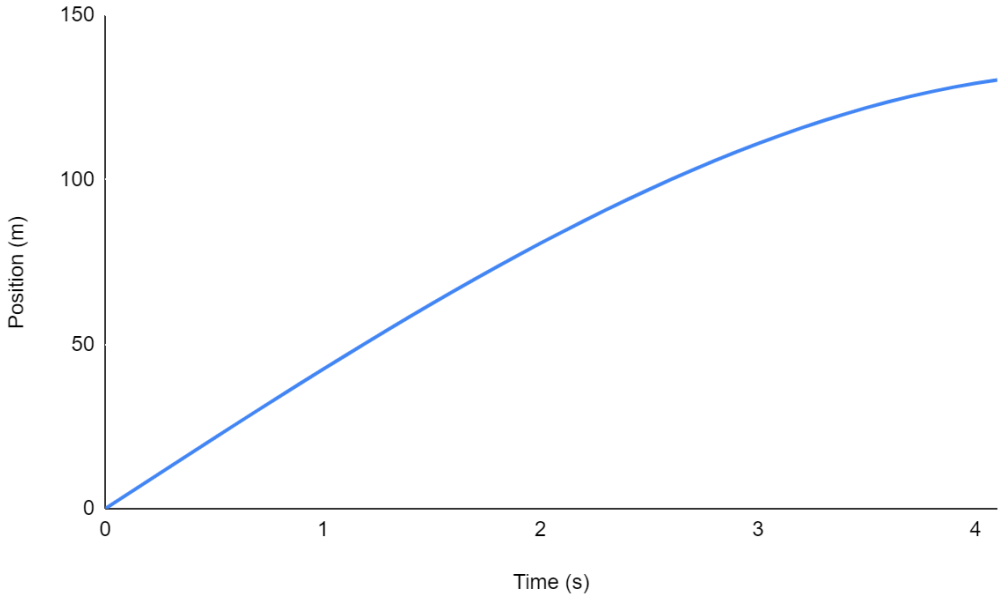

Figure 17: Plot of position over time for equation derivation of deceleration.

3.4 Fuel Cell Design

When designing a fuel cell, a current density must be chosen that best suits the needs of the application. For automotive purposes, a balance must be struck between a high

enough voltage and power. A low current density results in a high voltage cell and a low power density, whereas a high current density results in low voltage and high-power density. Therefore, for a hydrogen-air PEMFC under the operating conditions of 70 ºC at atmospheric pressure, a current density of 0.55 A cm^{-2} was selected. The polarization curve in Figure 18 below reveals that under the operating conditions, the corresponding voltage would be 0.64 V. The power density is simply the product of current density and voltage (Datta, 2020; Spiegel, 2007).

$$P = i \cdot V = (0.55\ A\ cm^{-2})(0.64\ V) = 0.352\ W\ cm^{-2} \quad (29)$$

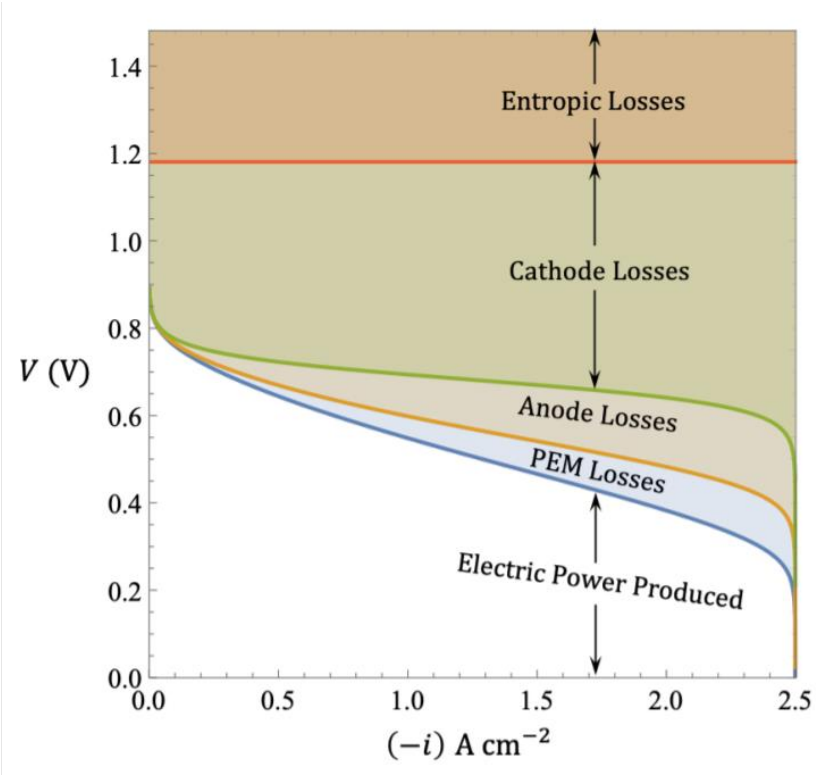

Figure 18: Polarization curve for a PEMFC at 70 ºC and atmospheric pressure demonstrating the various sources of potential drop (Datta R., 2020).

The efficiency of the fuel cell can be calculated to be 43% by the following equation:

$$\eta = \frac{0.64\ V}{1.482} = 0.43 \tag{33}$$

According to SAE regulations, the battery (or in our case the fuel cell) cannot supply more than 80 kW of power (SAE International, 2020). Thus, the required active area is the total power divided by the power density of a single cell.

$$A_{act} = \frac{P_{gross}}{P} = \frac{80{,}000\ W}{0.352\ W\ cm^{-2}} = 227.3\ cm^2 \tag{34}$$

To comfortably fit inside a standard SAE car, it was decided that the area of a single cell should be 40 cm wide by 10 cm long. Each cell had a thickness of 0.1 cm. Thus, the volume of a single cell is 40 cm^3. To calculate the number of cells, the total active area was divided by the area of the cell to give the number of cells.

$$N_{cells} = \frac{A_{act}}{A_{cell}} = \frac{227.27\ cm^2}{400\ cm^2\ cell^{-1}} = 568.2\ cells \tag{35}$$

The actual number of cells should be rounded up from the value calculated above. Thus, our fuel stack will end up having 569 cells.

The actual current of the fuel cell was determined by multiplying the current density by the cell area.

$$I = A_{cell} i = (400\ cm^2)(0.55\ A\ cm^{-2}) \tag{36}$$

The actual operating voltage of the fuel cell was determined by multiplying the voltage of a single cell by the total number of cells in the fuel stack (Datta, 2020; Spiegel, 2007).

$$V_{stack} = N_{cells} V_{cell} = (569)(0.64\ V) = 364.2\ V \tag{37}$$

$$Mass_{stack} = (569\ cells)(1513.5\ kg\ m^{-3})(0.000004\ m^3) \tag{38}$$

$$= 34.4\ kg$$

The flow rate of reactant and product species is calculated directly from the current. A utilization factor *S* is applied to flow rates since it is common practice to supply the fuel cell with more hydrogen than is consumed. A common utilization factor is 1.05 (Spiegel, 2007). Thus, the mass balances for the reactants and products are:

$$m_{H_2} = S\frac{I}{2F}M_{H_2}N_{cells} \tag{39}$$

$$m_{O_2} = S\frac{I}{4F}M_{O_2}N_{cells} \tag{40}$$

$$m_{H_2O} = S\frac{I}{2F}M_{H_2O}N_{cells} \tag{41}$$

In the case of our design, the fuel cell is not being supplied directly by pure oxygen, but rather by air which has a mass concentration of oxygen at 23%. Thus, it is useful to know the mass flow rate of air into the fuel cell, which is supplied by the following equation:

$$m_{air} = \frac{S}{x_{O_2}}\frac{I}{4F}M_{air}N_{cells} \tag{42}$$

The mass of our cell was approximated by using the fuel cell in the Toyota Mirai as a reference. The mass of the Toyota Mirai fuel cell is 56 kg and its volume is 37 L (0.037 m^3). Thus, we calculated the density of the Mirai fuel cell to be 1513.5 kg/m^3. Then, assuming that our fuel cell was of the same density as the current Mirai model, we calculated the mass of a single cell by multiplying the volume of the cell by density. Then the mass of the stack was calculated by multiplying the mass of the cell by the number of cells (2022 Toyota Mirai Specs & Options).

$$Mass_{stack} = N_{cells} \cdot \rho_{Mirai} \cdot Vol_{cell} \tag{43}$$

$$Mass_{stack} = (569\ cells)(1513.5\ kg\ m^{-3})(0.000004\ m^3) \quad (44)$$

$$= 34.4\ kg$$

The tank was sized by first determining how much hydrogen is required for a one-hour trip at full power which gives enough power for multiple laps around a track. By multiplying the molar flow rate of hydrogen consumed by the duration of one hour, we calculated the total amount of moles required to be stored in a full tank of compressed hydrogen. The tank is designed to be compressed at 75 MPa at 30 ºC (while the effect of temperature on highly compressed gasses is rather small, a worst-case scenario of a hot summer day was used to account for the volume of hydrogen). To calculate the volume of hydrogen, the Redlich-Kwong equation of state was used.

$$\left(P + \frac{a}{\bar{V}(\bar{V}+b)T^{1/2}}\right)(\bar{V}-b) = RT \quad (45)$$

$$a = 0.42748R^2\frac{T_c^{2.5}}{P_c} \quad (46)$$

$$b = 0.0.8664R\frac{T_c}{P_c} \quad (47)$$

The critical temperature and pressure of hydrogen were looked up as literature values. The variable $\bar{V}$ is the molar volume of hydrogen. To determine the actual volume of the tank, the molar volume was multiplied by the total number of moles required for one hour. Then the mass of the tank was determined by adding the mass of a titanium shell that is 0.01 m thick around the volume of hydrogen (Spiegel, S. Collen, 2007).

3.5 Fuel Cell Experimentation

The fuel cell of choice for this project was a PowerPEM-PS250 Fuel Cell from a previous major qualifying project completed at WPI in 2003 as seen below in Figure 19. Since fuel cells are often expensive and not easily obtainable, we chose to use this fuel cell for convenience. This fuel cell is a Solid-State PEM with a max output of 250 Watts. The fuel cell runs with ambient air and pure hydrogen (Seifert, 2004). The stack of the fuel cell contains 40 cells which theoretically produce 0.7 V per cell and has a total membrane area of 5680 cm^2 (Seifert, 2004). All assumptions and parameters in our experiments were made based on the previous work on this fuel cell as outlined above.

Figure 19: Front view of the PowerPEM-PS250 fuel cell used for experimentation

We experimented with the fuel cell at various current values to determine a polarization curve for the fuel cell and determine the optimal operating conditions to run the fuel cell such that it produces the highest power. Temperature measurements were also made to understand the effects of heating and cooling change on the fuel cell.

Once we powered the fuel cell air pumps and solenoids using an external 12 V source, the system was then attached to an electronic load to simulate the resistance of a motor which the fuel cell would be powering. After performing the necessary safety procedures, including leak testing, and pressurizing the system, we ran the fuel cell with hydrogen first at a constant pressure of 40 psi. While varying the current values we obtained a polarization curve for the fuel cell. Afterwards, we experimented with the temperature of the stack since it effects the overall performance of the fuel cell. According to the previous groups' work on this fuel cell, the fans used to cool the system were not used so the temperature was monitored and restricted to 80 °C to prevent the deterioration of the membrane. We were, however, able to get the fans working when we connected them to a separate external power source. We measured temperature and voltage as a function of time then plotted them on a graph to determine which temperature was optimal for running the fuel cell without any cooling; then we repeated this process for the system with cooling fans turned on.

4 RESULTS

4.1 The Fuel Cell Vehicle Design Tool (FCVDT)

The primary final deliverable of this project is the Fuel Cell Vehicle Design Tool, a MATLAB-based tool (see Appendix C) that provides necessary calculations for determining an SAE electric vehicles or similar type of vehicle's performance based on the design of the vehicle's fuel cell and battery powertrain. At the start of the code several inputs are required including the size of the track, the vehicle specifications (chassis mass, physical resistance coefficients, and wheel size), motor specifications (for gross power output), the design of the fuel cell (electric operations specifications, and the maximum operating time), and the battery specifications (percent allocation, energy density, and maximum operating time). The code then calculates the total mass of the vehicle from the mass of the fuel cell system, the mass of the battery, and the mass of the chassis. The mass and gross power then feed into the kinematic functions which each output data on the time, required power, power output, velocity, and acceleration. The data is then compiled and interpolated into a set of functions that are plotted in the output.

To calculate the effect of hybridization with a battery, the hybrid input must be switched on (by setting the Boolean to true) as well as setting the percent power allocation to the battery. This splits the total power output by such that a set percent of the power is supplied by the battery and the remaining from the fuel cell. The addition of the battery affects the total mass of the vehicle, thus changing the on-track performance of the vehicle.

From the power plots, the code integrates the data to find the total done. This value is compared to maximum available work from the fuel cell. Additionally, if the hybrid

Boolean is enabled to true, then code will calculate how much of the maximum available work is allocated to charging the battery and running the motor off the battery and fuel cell (individually and in combination). This was calculated with the assumption that the power distribution system between the fuel cell, battery, and motor is a series-parallel design.

This tool can be used by SAE teams or similar challenges to calculate the effects of changing parameters in the powertrain whether the design of the fuel cell, battery, or vehicle is their design process.

4.2 Sample Data Set From MATLAB

To demonstrate the capabilities of the tool, a basic test of keeping input variables constant while comparing performance results from hybridization to fuel cell only powertrain was compared. The input variables chosen to represent a realistic/potential racing condition.

The following inputs were made for a full fuel cell powered vehicle:

- Track parameters:
    - Radius of Turn: 25 m
    - Length of Straight Away: 800 m
- Vehicle Specifications:
    - Mass of Driver: 80 kg
    - Mass of Chassis: 250 kg
    - Frontal Area: 0.5 m^2
    - Coefficient of Drag: 0.27

    - Coefficient of Rolling Resistance Between Rubber Tires and Asphalt Road: 0.03
    - Static Coefficient of Resistance Between Rubber Tires and Asphalt Road: 0.7
    - Drivetrain Efficiency: 0.85
    - Minimum Braking Distance from 100 to 0 km/h: 30 m
    - Wheel and Tire Outer Diameter: 16”
    - Acceleration Jerk: 0.5 m/s^3
    - Braking Jerk: 4 m/s^3
- Motor Specifications:
    - Peak Power: 80 kW
    - Peak Torque: 230 Nm
- Fuel Cell:
    - Maximum Operating Time: 5 h
    - Cell Voltage: 0.64 V
    - Current Density: 0.55 A*cm^-2
    - Power Density: 0.352 W*cm^-2
    - Width of Cell: 40 cm
    - Length of Cell: 10 cm
    - Thickness of Cell: 0.1 cm
    - Fuel Cell Efficiency: 0.43
    - Ratio of Cell Active Area and Bipolar Plate: 0.7
    - Thickness of End Plates: 0.2 cm

The size of the track was selected such that it is close to 1 mile in total length. Vehicle and motor specifications were chosen to be realistic to an SAE or similar sized electric vehicle. The fuel cell design was selected such that it meets the power output requirements of the motor while fitting within the bounding area of an SAE or similar sized vehicle. The two variables that could be further developed (but serve as a base approximation for development purposes) is acceleration and braking jerk. Jerk, which is further explained in the methodology, was arbitrarily determined such that the time to maximum velocity was realistic and so that the peak power is reached at the vehicle output. This method could also be done in practice. However, in theory this value could be determined by throttle mapping. This is may even be especially easier with an electric vehicle since the system is drive by wire. Therefore, the mapping or programming for throttle response must be determined at some point. The same concept applies to braking jerk (without concern for peak power at the vehicle output).

These inputs resulted in a total mass of 390 kg (including the driver) and a lap time of 52.854 s. Because the fuel cell was the only power source, the power output is 80 kW with a total available work of 400 kWh from the 5 hours of hydrogen supply. The total work from one lap was 401 Wh, which means that the amount of available power consumption used was 0.1%. With one lap being approximately one mile, this means that the total range (at the speeds completed on this track) is roughly 1000 miles. This is not unrealistic considering that the energy density of hydrogen is roughly 3 times that of gasoline. Additionally, the weight of the vehicle is considerably low at 400 kg compared to the Toyota Mirai which has a curb weight of approximately 2000 kg and a range of 400

miles (Toyota Mirai Specs & Options, 2021). The console output can be seen in Appendix A.

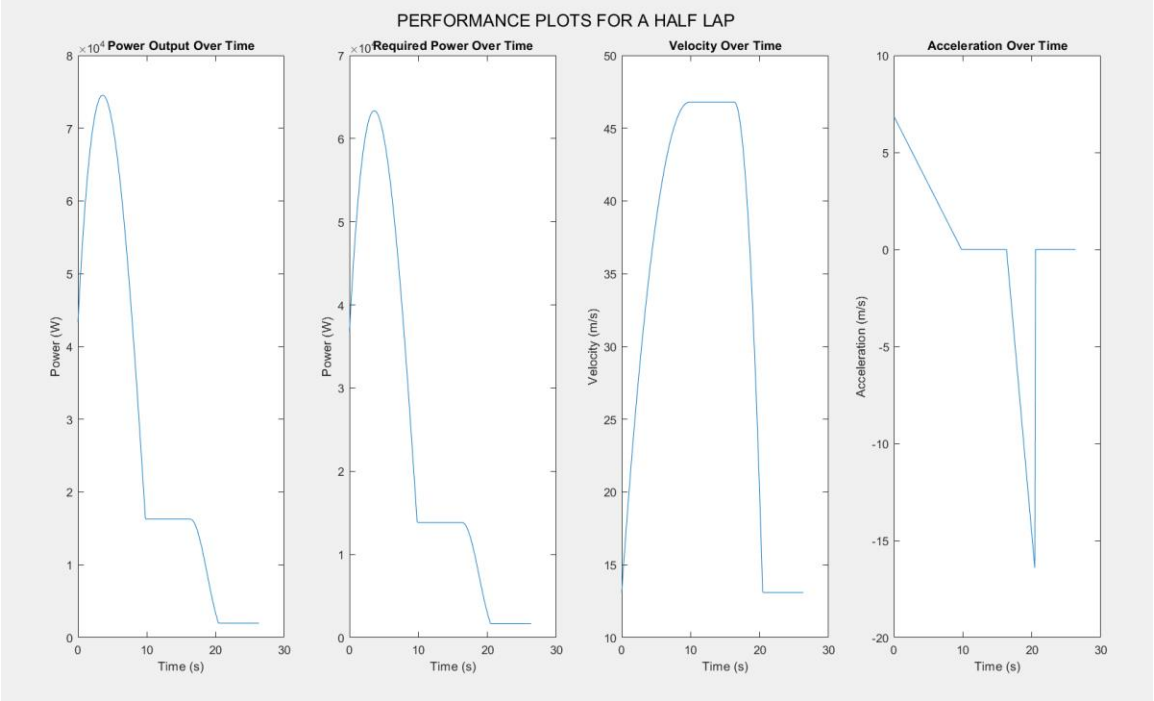

Figure 20: Vehicle Performance Plots from FCVDT for No Hybridization.

For the hybrid comparison, the same inputs were kept constant while adding a 10% power allocation to the battery with a maximum operating time of 1 hour at peak power (for the battery) and 265 Wh/kg energy density. The result was a total mass of 417 kg (including the driver) and a lap time of 52.854 s. The 10% power allocation means that the maximum power output from the fuel cell was 72 kW and the maximum power output from the battery was 8 kW. The total available work from 1 hour of battery supply and 5 hours of hydrogen supply was 368 kWh. The percent of battery's maximum work used is 0.052% and 0.28% for the fuel cell. The console output can be seen in Appendix B.

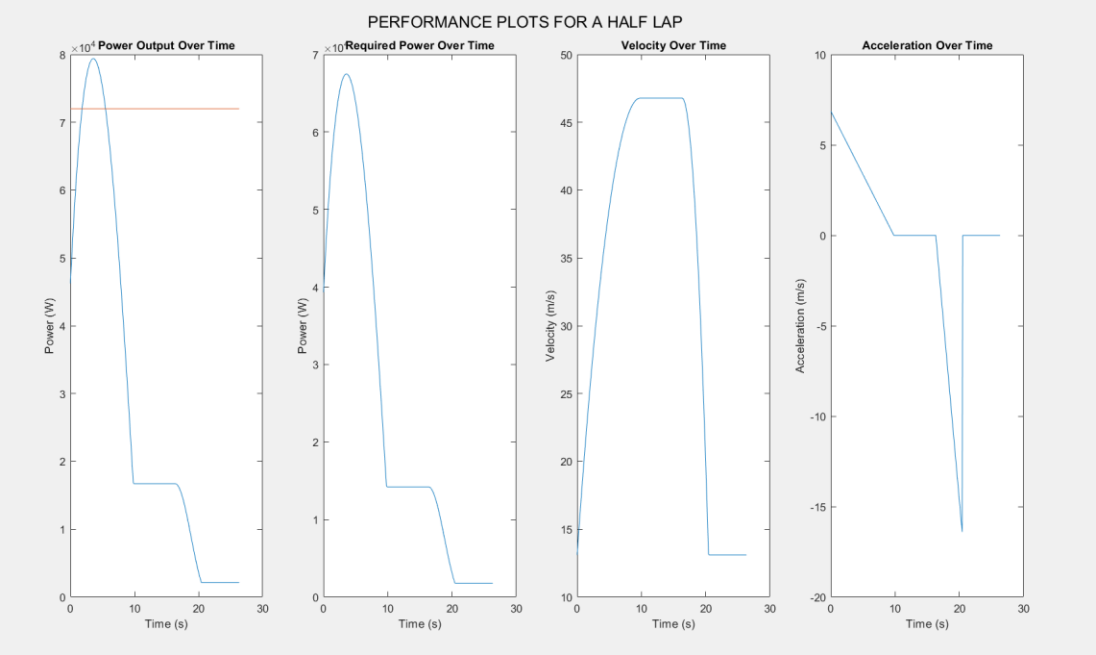

Figure 21: Vehicle Performance Plots from FCVDT for Hybridization.

Even with the increased weight from introducing in the battery to the system the lap time showed no change which is likely due to the reduction in power from fuel cell that is compensated with the battery. The major difference between the non-hybridization and hybridization is the power delivery. With non-hybridization the motor demand is supplied completely from the fuel cell. As shown by the blue line in the power output plot for no hybridization in Figure 20, the output is highly fluctuating, which is not good for the fuel cell, since they nominally operate at steady state. In the hybridization power output plot in Figure 21, the power from the fuel cell is held constant at the red line. From the starting point to the first intersection of the curves the fuel cell is charging the battery and powering the motor. Between two intersection points, the fuel cell powering the motor with assistance from the battery. Then from the second intersection point to the end, the fuel cell is powering the motor and charging the battery. This allows there to be no power

fluctuations from the output of the fuel cell. Keeping the power output of the fuel cell constant puts less strain on the system. All power fluctuations are handled by the battery which occur where more power is required.

Enabling and disabling hybrid calculation provides an additional design parameter that a user might need whether for performance benefits or race requirements in fuel cell vehicle design. An additional feature in the code is the ability to check if the hybrid change over contributes to the power output for the specific scenario. This line needs to intersect the power output curve for the battery to be useful for the application. If the percent battery is too low the hybrid change over line will be above the power output curve meaning that the battery will never kick in and is useless for the specific application.

If more power is allocated to the battery, then total mass increases at a faster rate than if more power is supplied to the fuel cell. This is because the energy density of lithium-ion battery is significantly lower than that of hydrogen. Furthermore, increasing the weight of the vehicle increases the lap time. This also means that any power allocation to the battery will increase the lap time. If the goal is also to mitigate power fluctuation from the fuel cell, then it makes sense have the hybridization with a low power allocation to the battery. This gives the fuel cell the benefit of constant output while not adding too much weight from the battery.

4.3 Experimental Results

To understand what currents would be appropriate for the physical fuel cell, we determined the polarization curve, shown below in Figure 22, based on the specifications of the fuel cell provided to us by the previous group's findings. We tested the fuel cell at

twenty different current values ranging from 0 to 9 amps. Each current was tested until peak voltage was reached. Then power was calculated from the voltage and current values. The voltage curve on Figure 22 yielded an increase in power and voltage around 8 amps, which was not expected. The slope of this curve should continue to decrease as the current increases. This could have been related to the fact that the fuel cell was not cooled well in between each data measurement set resulting in skewed results.

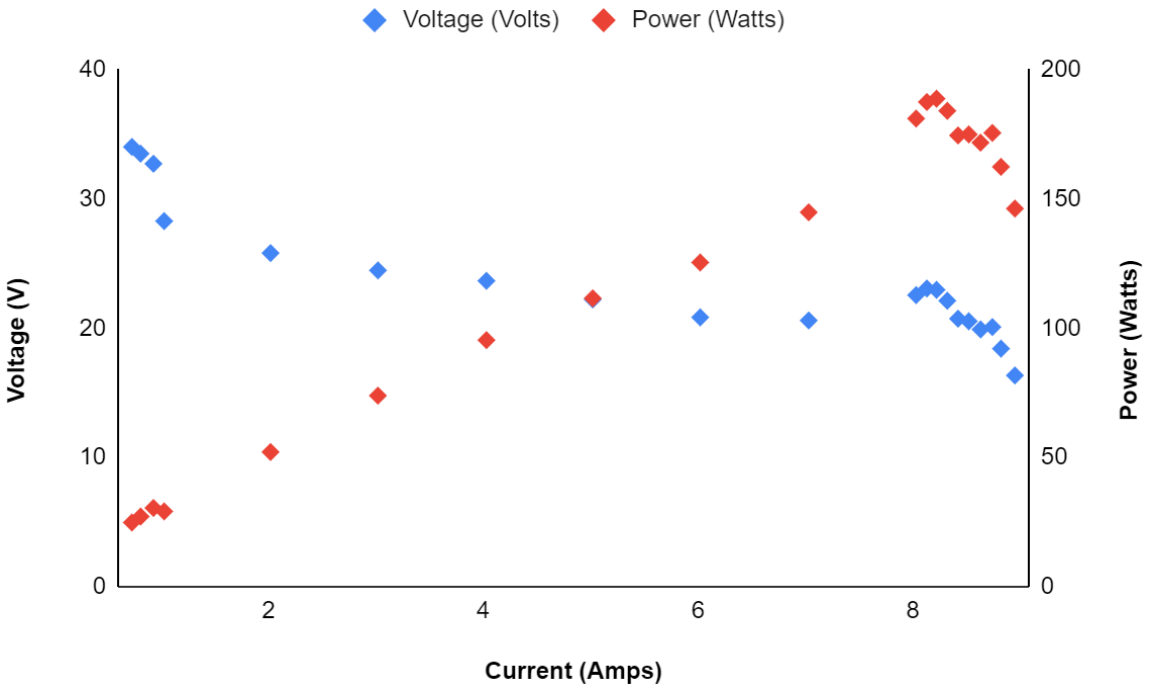

Figure 22: Polarization curve of PowerPEM-PS250 Fuel Cell at ambient operating pressure and 19 °C with an inlet hydrogen pressure of 40 psi. See Appendix D.1. for data behind this graph

After obtaining a polarization curve of known voltage, the fuel cell was tested to understand how heat management and temperature affect the performance of the fuel cell. The parameter that was varied in these experiments to test different loads on the cell was the current. Voltage and temperature were measured based on the current selected. As the current was increased, peak power and temperature also increased. The team observed that

the peak power for a specified current was not reached if the overall heating coefficient was smaller than the initial designed one. As seen in Figure 23 shown below, when the current was set to 8.03 amps with no cooling system, the fuel cell was unable to reach its maximum power. The introduction of fans powered at 5 V showed an increase in the power. This power was sustained over a longer period, but the temperature was not maintained throughout this process. With the 12V fan that the stack was designed with, the fuel cell performed the best. The peak power was reached and the temperature was stable, hence the system reached equilibrium.

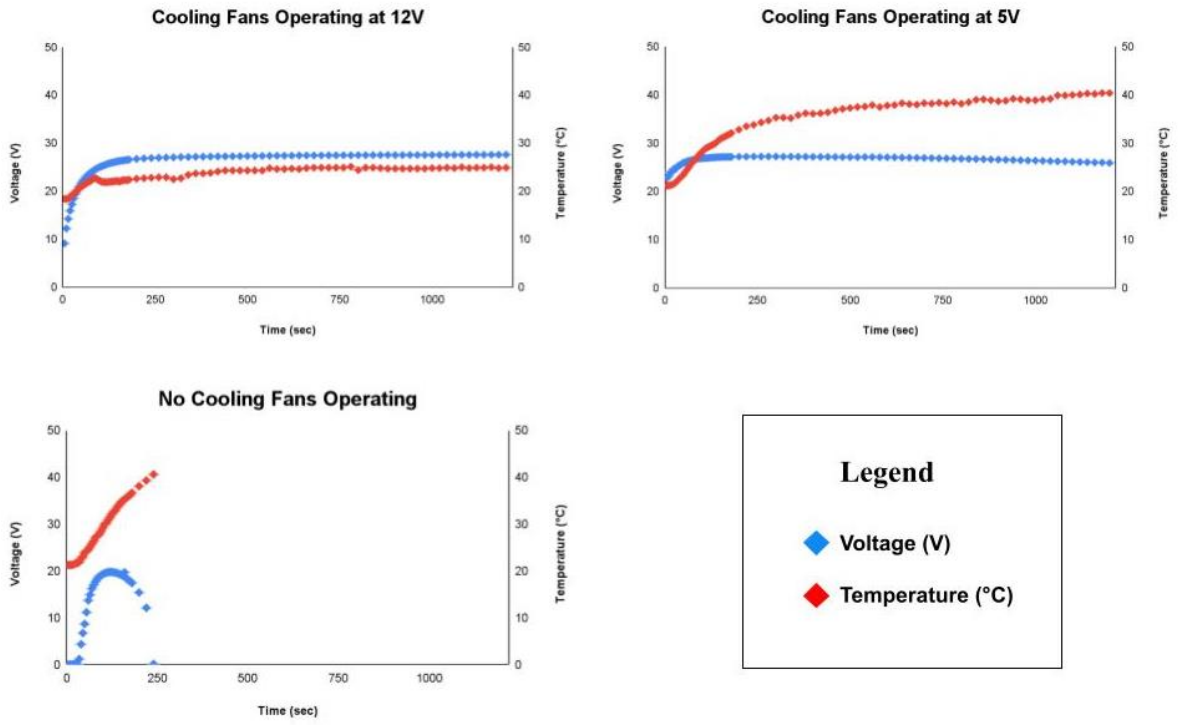

Figure 23: Voltage and temperature of the fuel cell over time operating at 8.03 amps.

When the fans were operating at 12 V, the data yielded even higher power outputs and the temperature was maintained at peak power. The peak power that was achieved from the fuel cell was 221.6 W. This process was repeated when the fuel cell was operating

at 5.02 A and 1.03 A. Tabulated data and graphs for these tests may be seen in Appendix D and Appendix E respectively. The results of these tests yielded lower power outputs as expected as well as similar relationships between temperature and power. It should be noted however, that when the fuel cell was tested on a lower current, the cooling fans at 12V hindered the performance of the stack. This effect could be caused by the fact that with such cooling the stack cannot get to the intended operating temperature. The lower fuel stack temperature only allowed a lower reaction rate, leading to a drop in power. Therefore, if stack needs to be used at lower currents, the cooling should be delayed or dampened until the temperature increases to what is needed for operation.

The group was also concerned in seeing the impacts of cooling into the performance efficiency of a fuel cell system. The experiment was operated at the same conditions the fuel cell was designed for, but the team reasoned that the fuel stack would have a decrease in efficiency due to the age of the fuel stack. First, the team needed to find the theoretical (or designed) power output and heat dissipation rates. The fuel stack was designed to produce 250 V peak power at 8 A. Knowing the peak power and operational current, the team was able to find the initial efficiency, named η_{th} *or theoretical efficiency*. The efficiency is simply a ratio of operating cell voltage and 1.23 V.

$$\eta_{th} = \frac{V}{1.23\ V} = \frac{\frac{250\ W}{8.0\ A} \cdot \frac{1}{40}}{1.23\ V} = 63.5\% \tag{48}$$

$$\eta_{th} = \frac{V}{1.23\ V} = \frac{\frac{250\ W}{8.0\ A} \cdot \frac{1}{40}}{1.23\ V} = 63.5\% \tag{49}$$

$$\Delta \dot{E}_{theoretical} = P_{theoretical} + \dot{Q}_{theoretical} = \frac{P_{theoretical}}{\eta} \tag{50}$$

$$\Delta\dot{E}_{theoretical} = 250\ W \cdot \frac{1.23\ V \cdot 40}{250\ W/_{8\ A}} = 393.6\ W$$

$$\begin{aligned}\dot{Q}_{theoretical} &= \Delta\dot{E}_{theoretical} - P_{theoretical} \\ &= 393.6\ W - 250\ W = 143.6\ W\end{aligned} \tag{51}$$

$$\Delta\dot{E}_{theoretical} = \Delta\dot{E}_{experimental} \tag{52}$$

$$\Delta \mathrm{P} = \Delta\dot{Q} \tag{53}$$

$$\mathrm{P_{theoretical}} - \mathrm{P_{experimental}} = \dot{Q}_{experimental} - \dot{Q}_{theoretical} \tag{54}$$

$$\begin{aligned}\dot{Q}_{experimental} &= \dot{Q}_{theoretical} - \mathrm{P_{experimental}} + \mathrm{P_{theoretical}} \\ &= 143.6\ W - 221.6\ \mathrm{W} + 250\ W \\ &= 172\ W\end{aligned} \tag{55}$$

With the known efficiency, the $P_{theoretical} + \dot{Q}_{theoretical}$ sum can be found where the sum equals the total amount of energy exerted from the fuel stack. The total energy is denoted as $\Delta\dot{E}_{theoretical}$ and will equal the energy released during our experiment. Hence, $\Delta\dot{E}_{theoretical} = \Delta\dot{E}_{experimental}$. This factor is true if the setup in the experiment is the same as what the fuel stack was designed to operate under (inlet H_2 pressure, inlet oxygen pressure, operating temperature). As mentioned above, the term "theoretical" describes the quantities and values during the first design and use of the fuel cell.

$$\eta_{th} = \frac{-\frac{\Delta_f G}{nF}}{-\frac{\Delta_f H}{nF}} = \frac{\Delta_f G}{\Delta_f H_{LHV}} = \frac{V}{1.23\ V} = \frac{P_{theoretical}}{P_{theoretical} + \dot{Q}_{theoretical}} \tag{49}$$

$$\Delta\dot{E}_{theoretical} = P_{theoretical} + \dot{Q}_{theoretical} = \frac{P_{theoretical}}{\eta} \tag{50}$$

$$\Delta\dot{E}_{theoretical} = 250\ W \cdot \frac{1.23\ V \cdot 40}{250\ W/_{8\ A}} = 393.6\ W$$

With the $\Delta\dot{E}_{theoretical} = 393.6W$, the designed heat rate dissipation could be found. In addition, the heat transfer rate during the experiment can be found.

$$\dot{Q}_{theoretical} = \Delta\dot{E}_{theoretical} - P_{theoretical} = 393.6\ W - 250\ W = 143.6\ W \quad (51)$$

$$\Delta\dot{E}_{theoretical} = \Delta\dot{E}_{experimental} \quad (52)$$

$$\Delta \mathrm{P} = \Delta\dot{Q} \quad (53)$$

$$\mathrm{P}_{\mathrm{theoretical}} - \mathrm{P}_{\mathrm{experimental}} = \dot{Q}_{experimental} - \dot{Q}_{theoretical} \quad (54)$$

$$\dot{Q}_{experimental} = \dot{Q}_{theoretical} - \mathrm{P}_{\mathrm{experimental}} + \mathrm{P}_{\mathrm{theoretical}} = 143.6\ W = 172\ W \quad (55)$$

$$\eta_{experimental} = \frac{P_{experimental}}{P_{experimental} + \dot{Q}_{experimental}} = \frac{221.6\ W}{221.6\ W + 172\ W} = 56.3\% \quad (56)$$

Finally, the new real efficiency was found. As seen above, the efficiency decreased with time, hence proving the team's suspicion as accurate.

5 CONCLUSION AND RECOMMENDATIONS

5.1 Outlook, Future Work, and Recommendations

This project set out to build a design tool that an SAE team or similar small scale vehicle race team could use to design fuel cell powered electric vehicle. However, there is certainly some room for future work to achieve more robust results. These include, but not limited to, the implementation of regenerative breaking and a heat management system into our model.

Regenerative breaking is a form of automotive energy conservation that allows for increased electric potential energy in the motor; as a vehicle slows down, the motor does not spin, but the wheels are still moving. Regenerative breaking converts the kinetic energy of the moving wheels to electric potential energy in the motor. This would be a good addition to our model from an efficiency point of view. With regenerative breaking, the vehicle in our model could require less fuel storage or even require a smaller battery, therefore decreasing the overall mass. The decreased mass of the vehicle would allow a lap to be completed in less time.

Our experimental work with the PowerPEM-PS250 Fuel Cell reinforced the idea that a cooling system is necessary to benefit the overall power output of the cell. From our findings at higher loads, the fuel cell needs better cooling to maintain a higher performance. We believe that with more research the right temperature can be maintained in order to run the fuel cell at maximum efficiency. The addition of a heat management system into our Fuel Cell Vehicle Design tool will improve the usability of our tool and allow for users to

incorporate more details of their vehicle with the overall goal of minimizing the time required to complete the race.

In addition to the above recommendations, our team advises the following:

- An optimal temperature associated with each current was observed. More research is needed to find what the optimal operating temperature is.
- Use the operating temperature measures to create a code that runs the cooling system at different capacities depending on the instantaneous temperature.
- Improve the vehicle dynamics MATLAB code with a more accurate acceleration model
- Research on different fuel types that may decrease weight, increase efficiency, and increase lifespan.
- Research ways to create an electrical circuit for the hybrid system.
- Develop a cost analysis for a first iteration HFC-Battery hybrid system

5.2 Conclusion

As businesses and industries look towards reducing environmental impacts, the automotive sector seeks to put an emphasis on innovation in this area. Fuel cells offer an alternate pathway in automotive applications to achieve similar, if not better outputs than EV and ICE vehicles. In recent years, fuel cell vehicles have gained traction due to their lack of greenhouse emissions and ecofriendly benefits. Engineers need appropriate tools to account for the effect of design changes on fuel cell vehicle's performance. The Fuel

Cell Vehicle Design Tool (FCVDT) that we have developed provides an initial step in creating tools for vehicle design and optimization.

REFERENCES

2022 Toyota Mirai Specs & Options. (2021). Retrieved December 12, 2021, from https://www.toyota.com/mirai/features/mpg_other_price/3002/3003.

Bagotsky, Vladimir S. (2012). *Fuel Cells: Problems and Solutions* (2nd ed.). John Wiley & Sons, Inc.

Bauen, A., & Hart, D. (2000). Assessment of the environmental benefits of transport and stationary fuel cells. *Journal of power sources*, *86*(1-2), 482-494.

C Iclodean et al 2017 IOP Conf. Ser.: Mater. Sci. Eng. 252 012058

Chen, Y.-S., Lin, S.-M., & Hong, B.-S. (2013). Experimental study on a passive fuel cell/Battery Hybrid Power System. *Energies*, *6*(12), 6413–6422. https://doi.org/10.3390/en6126413

Datta, R. (2020). *Fuel Cells and Hydrogen. Science and Technology* (Chapter 5. The Basic Fuel Cell Model). Unpublished Manuscript

Dicks, A. L., & Rand, D. A. J. (2018). *Fuel Cell Systems Explained.* (3rd ed.). John Wiley & Sons, Ltd.

Gambir, R., & Jha, A. K. (2013, May 5). *Brushless DC Motor: Construction and Applications*. Retrieved from https://www.theijes.com/papers/v2-i5/Part.3/K0253072077.pdf

He, Y., Miao, C., Wu, J., Zheng, X., Liu, X., Liu, X., & Han, F. (2021). Research on the power distribution method for hybrid power system in the Fuel Cell Vehicle. *Energies*, *14*(3), 734. https://doi.org/10.3390/en14030734

Larmine, James & Dicks, Andrew. (2003). *Fuel Cell Systems Explained*. (2nd ed.). John Wiley & Sons, Lmt.

Lototskyy, M. V., Tolj, I., Pickering, L., Sita, C., Barbir, F., & Yartys, V. (2017). The use of metal hydrides in fuel cell applications. Progress in Natural Science: Materials International, 27(1), 3-20.

Ma, S., Lin, M., Lin, T.-E., Lan, T., Liao, X., Maréchal, F., Van herle, J., Yang, Y., Dong, C., & Wang, L. (2021). Fuel cell-battery hybrid systems for mobility and off-grid applications: A Review. *Renewable and Sustainable Energy Reviews*, *135*, 110119. https://doi.org/10.1016/j.rser.2020.110119

Panayiotou, Gregoris & Kalogirou, Soteris & Tassou, Savvas. (2010). PEM Fuel Cells for Energy Production in Solar Hydrogen Systems. Recent Patents on Mechanical Engineering. 3. 226-235. 10.2174/2212797611003030226.

SAE International. (2020, July 30). Formula SAE Rules 2021. Formula SAE. Retrieved August 30, 2021, from https://s3.us-west-2.amazonaws.com/secure.notion-static.com/1b2d3502-78a9-4707-83dd-80f868071b49/FSAE_Rules_2021_V1.pdf?X-Amz-Algorithm=AWS4-HMAC-SHA256&X-Amz-Content-Sha256=UNSIGNED-PAYLOAD&X-Amz-Credential=AKIAT73L2G45EIPT3X45%2F20211212%2Fus-west-2%2Fs3%2Faws4_request&X-Amz-Date=20211212T035139Z&X-Amz-Expires=86400&X-Amz-Signature=13429693419f927c0cc2398bcd4fcea7bd02802fc967d2bbdcb523cd311b05a2&X-Amz-SignedHeaders=host&response-content-disposition=filename%20%3D%22FSAE_Rules_2021_V1.pdf%22&x-id=GetObject

Seifert, N., LaPointe, J., Matara, J., & Elolampi, B. (2004). *Fuel cell powered scooter*. Worcester Polytechnic Institute.

Spiegel, S. Collen. (2007). *Designing and Building Fuel Cells*. McGraw-Hill

Spiegel, C. (2017, June 6). Fuel Cell Characterization. Fuel Cell Store. Retrieved December 19, 2021, from https://www.fuelcellstore.com/blog-section/fuel-cell-characterization

Vielstich, W., Lamm, A., Gasteiger, H. A. (2003) *Handbook of Fuel Cells - Fundamentals, Technology, and Applications*. (Vol. 3-4). John Wiley & Sons, Ltd.

APPENDIX A: FCVDT TEST RESULTS WITHOUT HYBRIDIZATION

FUEL CELL VEHICLE DESIGN TOOL

Power Source: Hydrogen Fuel Cell

ON TRACK PERFORMANCE INFO BY SECTION
Section 1 | v2 = 46.7851 m/s | a1 (max) = 6.867 m/s^2 | t1 = 9.8 s | l1 = 348.3519 m | P1 (max output) = 74536.7827 W
Section 2 | t2 = 6.5358 s | l2 = 305.7766 m | P2 (const output) = 13842.1241 W
Section 3 | a3 (max) = 0 m/s^2 | t3 = 4.1 s | l3 = 145.8715 m
Section 4 | v4 = 13.1025 m/s | a4 (const) = 0 m/s^2 | t4 = 5.9912 s | l4 = 78.5 | P4 (const output) = 1989.5972 W

TRACK INFO
Total Track Length = 1757 m

TRACK FINAL RESULTS
Calculated Lap Time = 52.854 s
Average Velocity = 33.2425 m/s

MASS INFO
Total Mass of Vehicle = 390.337 kg
Mass of FC Stack = 34.4476 kg
Mass of FC Tank = 25.8894 kg
Mass of Battery = 0 kg
Mass of Chassis = 250 kg
Mass of Driver = 80 kg

POWER INFO
Maximum Power Output of Fuel Cell = 80000 W
Available Work From Fuel Cell = 400000 Wh
Total Work Done = 401.4113 Wh
Percent of Total Work Used = 0.10035%

APPENDIX B: FCVDT TEST RESULTS WITH HYBRIDIZATION

FUEL CELL VEHICLE DESIGN TOOL

Power Source: Hydrogen Fuel Cell Hybridization with Battery

ON TRACK PERFORMANCE INFO BY SECTION
Section 1 | v2 = 46.7851 m/s | a1 (max) = 6.867 m/s^2 | t1 = 9.8 s | l1 = 348.3519 m | P1 (max output) = 79396.7242 W
Section 2 | t2 = 6.5358 s | l2 = 305.7766 m | P2 (const output) = 14210.2738 W
Section 3 | a3 (max) = 0 m/s^2 | t3 = 4.1 s | l3 = 145.8715 m
Section 4 | v4 = 13.1025 m/s | a4 (const) = 0 m/s^2 | t4 = 5.9912 s | l4 = 78.5 | P4 (const output) = 2110.8946 W

TRACK INFO
Total Track Length = 1757 m

TRACK FINAL RESULTS
Calculated Lap Time = 52.854 s
Average Velocity = 33.2425 m/s

MASS INFO
Total Mass of Vehicle = 417.0749 kg
Mass of FC Stack = 30.9968 kg
Mass of FC Tank = 25.8894 kg
Mass of Battery = 30.1887 kg
Mass of Chassis = 250 kg
Mass of Driver = 80 kg

POWER INFO
Maximum Power Output of Fuel Cell = 72000 W
Available Work From Fuel Cell = 360000 Wh
Maximum Power Output of Battery = 8000 W
Maximum Available Work From Battery = 8000 Wh
Total Available Work = 368000 Wh
Total Work Done = 1063.4309 Wh
Work From BAT + FC = 156.2637 Wh
Work From FC Charging BAT = 639.8825 Wh
Work From BAT = 10.0001 Wh
Work From FC = 1053.4308 Wh

Percent of BAT Used = 0.125 %
Percent of FC Used = 0.29262 %
Percent of Total Work Used = 0.28898%

APPENDIX C: FCVDT MATLAB CODE

```
%MATLAB: Fuel Cell Vehicle Design Tool
%
%DESCRIPTION: based on design inputs for vehicle and fc electric powertrain, code calculates
vehicle's on track performance. the model is for an indy style
%race track. Requires symbolic math tool box and mapping toolbox
%
%LAST MODIFIED: Tyler Vu - 12/15/2021.

%closes any open figures and clears workspace
close all
clear

%%%%%%DESIGN INPUTS%%%%%%

%TRACK PARAMETERS
r = 12; %turn radius (m)
L = 800; %straight away length (m)

%VEHICLE SPECS
mDriver = 80; %driver weight (kg)
mChassis = 250; %mass of vehicle (kg)
A = .5; %frontal area (m^2)
cd = .27; %drag coefficient
crr = .03; %friction coefficient between tire and road
csr = 0.7; %static friction coefficient between tire and road
driveEff=0.85; %drivetrain efficiency

wheelR = .203; %wheel and tire radius (m)
accelJerk = 0.70; %throttle mapping rate of acceleration (m/s^3)
brakeJerk = 4; %rate of decceleration (m/s^3)

%MOTOR SPECS
pMotor = 80000; %motor power (W)
tMotor = 230; %peak torque (N/M)

%FUEL CELL DESIGN
fcOpTime = 5;  %max operation time at peak power (s)
v=0.64;                % cell voltage
i=0.55;                % current density                  (Acm^-2)
p=0.352;               % power density                    (Wcm^-2)
w=40;                  % width of cell (cm)
l=10;                  % length of the cell (cm)
Efc= .43;              % Efficiency of the fuel cell
dcell=0.1;            % Thickness of the cell (cm)
alphact=0.7;            % Ratio of cell active area and bipolar plate area
Dep=0.2;                %thickness of end plates (cm)

%HYBRID CONSIDERATION
hybrid = false; % enables (true) and disables (false) hybrid calculations
pctBattery = 0.30; % percent power allocation to battery
batteryEnergyDensity = 265; % Wh/kg
batOpTime = 1; %max op time at peak power

%GENERAL PHYSICS/CHEM PARAMETERS
g = 9.81;              %gravity (kg*m/s^2)
rho =1.225;            %density of air (kg/m^2)
F=96485.3329;          %Farady Constant
Mh2=2.02;              % Molar mass of H2                  (g/mol)
Mo2=32.02;             % Molar mass of O2                  (g/mol)
Mh2o=18.04;            % Molar mass of water               (g/mol)
Mair=28.97;            % Molar mass of air                 (g/mol)
xo2=0.21;               % Molar frac of O2 in air
Psat= 0.308;            % saturated pressure of water @ 70C
phi_an=.70;
P_an=1;                 % These 4 to be changed
```

```
phi_ca=.70;
P_ca=1;

%%%%%%OUTPUTS AND DATA INTERP%%%%%%

%adjusts power of sources if hybrid is enabled
if hybrid == true
    batPwr = pMotor * pctBattery;
    fcPwr = pMotor * (1-pctBattery);
    mBattery = (batPwr*batOpTime)/batteryEnergyDensity;
else
    fcPwr = pMotor;
    mBattery = 0;
    batPwr = 0;
end

% calculates max available power consumption Wh
batMaxWork = batPwr * batOpTime;
fcMaxWork = fcPwr * fcOpTime;
totalMaxWork = batMaxWork + fcMaxWork;

%displays track in figure 1
figure(1)
trackVar = imshow('Track Variables.jpg');

%runs fc design
[mStack, mTank] = fuelCellDesign(fcOpTime, F, Mh2, Mo2, Mh2o, Mair, xo2, Psat, phi_an, P_an,
phi_ca, P_ca, v, i, p, fcPwr, w, l, Efc, dcell, alphact, Dep);

%calculates total vehicle mass
mTank = double(mTank);
mVehicle = mDriver + mChassis + mStack + mTank + mBattery;

%runs vehicle performance calculations by section
[v4,t4, P4, l4, timeSection4, preqSection4, poutSection4, velSection4, accelSection4] =
sec4(csr,crr,g,r, mVehicle, cd, A,driveEff);
[v2,t1,P1,a1,l1, timeSection1, preqSection1, poutSection1, velSection1, accelSection1] =
sec1(g,rho,mVehicle,csr,crr, v4, cd,A,driveEff, pMotor, tMotor, wheelR, accelJerk);
[t3,l3,a3, timeSection3, preqSection3, poutSection3, velSection3, accelSection3] = sec3(brakeJerk,
v4,v2,mVehicle,g,crr,rho,A,cd);
[l2,t2,P2, timeSection2, preqSection2, poutSection2, velSection2, accelSection2] =
sec2(v2,L,l1,l3,mVehicle,g,crr,cd,A,driveEff);

%combines performance data from sections
timeSection2 = timeSection2 + t1;
timeSection3 = timeSection3 + t1 + t2;
timeSection4 = timeSection4 + t1 + t2 + t3;
time = [timeSection1, timeSection2, timeSection3, timeSection4];
powerReq = [preqSection1, preqSection2, preqSection3, preqSection4];
powerOut = [poutSection1, poutSection2, poutSection3, poutSection4];
velocity = [velSection1, velSection2, velSection3, velSection4];
acceleration = [accelSection1, accelSection2, accelSection3, accelSection4];

%outputs plots for half lap
figure(2)
sgtitle('PERFORMANCE PLOTS FOR A HALF LAP');

%Power Output interp and plot
powerOutInterp = griddedInterpolant(time,powerOut); %interpolate Pout dataset
powerOutFunction = @(time) powerOutInterp(time); %creates function from interpolated data
subplot(1,4,1);
plot(time,powerOutFunction(time));
title("Power Output Over Time");
xlabel("Time (s)");
ylabel("Power (W)");

%plots hybrid change over line and calculates related power consumption values
if hybrid == true
```

```
    hold on
    for i = 1:length(time)
        hybridLine(i) = pMotor * (1-pctBattery);
    end
    hybridLineInterp = griddedInterpolant(time,hybridLine); %interpolate Preq dataset
    hybridLineFunction = @(time) hybridLineInterp(time); %creates function from interpolated data
    plot(time,hybridLineFunction(time));
    hold off

    intersect = polyxpoly(time,powerOutFunction(time),time,hybridLineFunction(time));
    if length(intersect)<2
        disp("Hybrid power change over line does not intersect total power output curve accross
two points. Code will throw error message.");
        disp("Increase the percent battery so that the hybrid line intersects the power output
curve.")
    else
        workBatPlusFC = 2*integral(powerOutFunction,intersect(1),intersect(2))/3600;
        workBat = 2*(integral(powerOutFunction,intersect(1),intersect(2))-
integral(hybridLineFunction,intersect(1),intersect(2)))/3600;
        workFC = 2*integral(hybridLineFunction,time(1),time(end))/3600;
        workFCChargeBat = 2*((integral(hybridLineFunction,time(1),intersect(1))-
integral(powerOutFunction,time(1),intersect(1)))+(integral(hybridLineFunction,intersect(2),time(en
d))-integral(powerOutFunction,intersect(2),time(end))))/3600;
        totalWorkDone = workFCChargeBat+(2*integral(powerOutFunction,time(1),time(end))/3600);
        pctBatUsed = 100*(workBat/batMaxWork);
        pctFCUsed = 100*(workFC/fcMaxWork);
    end
else
    totalWorkDone = 2*integral(powerOutFunction,time(1),time(end))/3600;
end

%calculates how much of the available consumption is used for 1 lap
pctAvailWorkUsed = 100*(totalWorkDone/totalMaxWork);

%Req Power Interp and Plot
powerReqInterp = griddedInterpolant(time,powerReq); %interpolate Preq dataset
powerReqFunction = @(time) powerReqInterp(time); %creates function from interpolated data
subplot(1,4,2);
plot(time,powerReqFunction(time));
title("Required Power Over Time");
xlabel("Time (s)");
ylabel("Power (W)");

% Velocity interp and plot
velocityInterp = griddedInterpolant(time,velocity); %interpolate vel dataset
velocityFunction = @(time) velocityInterp(time); %creates function from interpolated data
subplot(1,4,3);
plot(time,velocityFunction(time));
title("Velocity Over Time");
xlabel("Time (s)");
ylabel("Velocity (m/s)");

% Acceleration interp and plot
accelInterp = griddedInterpolant(time,acceleration); %interpolate accel dataset
accelFunction = @(time) accelInterp(time); %creates function from interpolated data
subplot(1,4,4);
plot(time,accelFunction(time));
title("Acceleration Over Time");
xlabel("Time (s)");
ylabel("Acceleration (m/s)");

% Command Window Outputs
disp(newline);

disp("FUEL CELL VEHICLE DESIGN TOOL");

disp(newline)
```

```
if hybrid == true
    disp("Power Source: Hydrogen Fuel Cell Hybridization with Battery");
else
    disp("Power Source: Hydrogen Fuel Cell")
end

disp(newline);

disp("ON TRACK PERFORMANCE INFO BY SECTION")
disp("Section 1 | v2 = " + string(v2) + " m/s | a1 (max) = " + string(a1) + " m/s^2 | t1 = " +
string(t1) + " s | l1 = " + string(l1) + " m | P1 (max output) = " + string(P1) + " W");
disp("Section 2 | t2 = " + string(t2) + " s | l2 = " + string (l2) + " m | P2 (const output) = " +
string(P2) + " W" );
disp("Section 3 | a3 (max) = " + string(a3) + " m/s^2 | t3 = " + string(t3) + " s | l3 = " +
string(l3) + " m");
disp("Section 4 | v4 = " + string(v4) + " m/s | a4 (const) = 0 m/s^2 | t4 = " + string(t4) + " s |
l4 = " + string(l4) + " | P4 (const output) = " + string(P4) + " W");

disp(newline);

%calculate total track legnth, laptime, and average velocity
trackLen = 2*(L+l4);
lapTime = 2*(t1+t2+t3+t4);
avgVel = trackLen/lapTime;

disp("TRACK INFO")
disp("Total Track Length = " + string(trackLen) + " m");

disp(newline);

disp("TRACK FINAL RESULTS");
disp("Calculated Lap Time = " + string(lapTime) + " s");
disp("Average Velocity = " + string(avgVel) + " m/s");

disp(newline);

disp("MASS INFO")
disp("Total Mass of Vehicle = " + string(mVehicle) + " kg");
disp("Mass of FC Stack = " + string(mStack) + " kg");
disp("Mass of FC Tank = " + string(mTank) + " kg");
disp("Mass of Battery = " + string(mBattery) + " kg");
disp("Mass of Chassis = " + string(mChassis) + " kg");
disp("Mass of Driver = " + string(mDriver) + " kg");

disp(newline);

disp("POWER INFO")
disp("Maximum Power Output of Fuel Cell = " + string(fcPwr) + " W");
disp("Available Work From Fuel Cell = " + string(fcMaxWork) + " Wh");
if hybrid == true
    disp("Maximum Power Output of Battery = " + string(batPwr) + " W");
    disp("Maximum Available Work From Battery = " + string(batMaxWork) + " Wh");
    disp("Total Available Work = " + string(totalMaxWork) + " Wh")
end
disp("Total Work Done = " + totalWorkDone + " Wh");
if hybrid == true
    disp("Work From BAT + FC = " + workBatPlusFC + " Wh");
    disp("Work From FC Charging BAT = " + workFCChargeBat + " Wh");
    disp("Work From BAT = " + workBat + " Wh");
    disp("Work From FC = " + workFC + " Wh");
    disp("Percent of BAT Used = " + pctBatUsed + " %");
    disp("Percent of FC Used = " + pctFCUsed + " %");
end
disp("Percent of Total Work Used = " + pctAvailWorkUsed + "%")
disp(newline)

%%%%%% FUNCTIONS %%%%%%
```

```
%%%FUEL CELL DESIGN%%%

function [mStack, mTank] = fuelCellDesign(operationTime, F, Mh2, Mo2, Mh2o, Mair, xo2, Psat,
phi_an, P_an, phi_ca, P_ca, v, i, p, Pgross, w, l, Efc, dcell, alphact, Dep)

    Acell=w*l;             % Area of a single cell              (cm^2)
    Vol_cell=w*l*dcell;    % cm3

    %Active Area, Number of Cells and Overall Voltage

    Aact= Pgross/p;
    Ncell=Aact/Acell;
    Ncelf=ceil(Ncell);
    I=Acell*i;
    V=Ncell*v;

    % Finding the Heat Lossed in the Fuel Cell

    Q=(1.29-v)*I*Ncelf;  % Use the 1.29

    % Mass Balances
    S=1.05;
    nh2=(I/(2*F));   %Molar Rates with units of mol/s
    no2=(I/(4*F));
    nh2o=(I/(2*F));

    % Inlet Mass flow Rate
    mh2=S*(I/(2*F))*Mh2*Ncelf;  %Units: g/s
    mo2=S*(I/(4*F))*Mo2*Ncelf;
    mh2o=S*(I/(2*F))*Mh2o*Ncelf;
    mair=(S/xo2)*(I/(4*F))*Mair*Ncelf;

    % Inlet Water Vapor Flow Rate
    mh2o_h2=S*(Mh2o/(2*F))*((phi_an*Psat)/(P_an-phi_an*Psat))*I*Ncelf;
    mh2o_o2=S*(Mh2o/(4*F))*((phi_ca*Psat)/(P_ca-phi_ca*Psat))*I*Ncelf;
    mh2o_air=(S/xo2)*(Mh2o/(4*F))*((phi_ca*Psat)/(P_ca-phi_ca*Psat))*I*Ncelf;

    %Mass of the fuel cell
    %% Using Toyota Mirai's density per cell to calculate the mass of the MQP's fuel Cell

    m_toyota=56;
    V_toyota=0.037;  % in m3

    pho_toyota= m_toyota/V_toyota;
    mcell=pho_toyota*(Vol_cell*10^(-6));
    mStack=mcell*Ncelf; %kg

    %Finding Volume of Hydrogen in the Tank
     P=75*10^6;  %Pa
     R=8.314; %m^3*Pa/mol*K
     T=303.15; %K
     Tc=33.2;  %K
     Pc=12.98*10^5;  %Pa                    % Tank Volume Vs Pressure
     a=0.42748*R^2*Tc^2.5/Pc;
     b=0.08664*R*Tc/Pc;

     Vm=roots([1  -R*T/P  a/(P*T^0.5)-b^2-b*R*T/P  -a*b/(P*T^0.5)]); %Redlich-Kwong EOS
     Vm=vpa(Vm(1)); %m^3/mol

    %Finding Volume of Hydrogen in the Tank: Iteration 2
    tlength=operationTime*3600;    %seconds
    molh2=nh2*tlength;
    massh2=molh2*2.02/1000;
    Vol_h2=Vm*molh2;  %m^3
    Vol_h2_L=Vol_h2*1000;  %L

    %Finding Mass of the Tank: Iteration 2
    %Tank Height
```

```
    r1=0.05; %m
    height_tank=(Vol_h2-(4/3)*3.14159*r1^3)/(3.14159*r1^2); %m
    %Dynamic Wall Mass
    rho_dyn=593; %kg/m^3
    r2=r1+0.05;
    Vol_dyn=(3.14159*r2^2+(4/3)*3.14159*r2^3)-Vol_h2;
    mass_dyn=Vol_dyn*rho_dyn; %kg
    %Titanium Wall Mass
    rho_Ti=7860; %kg/m^3
    r3=r2+0.01;
    Vol_dyn=(3.14159*r3^2+(4/3)*3.14159*r3^3)-Vol_dyn;
    mass_Ti=Vol_dyn*rho_dyn; %kg
    %Tank Total Mass
    mTank=massh2+mass_dyn+mass_Ti;
    %Percent Fraction of Hydrogen:Tank
    percent_frac_H2_Tank=100*massh2/mTank;

end

%%%VEHICLE KINEMATICS FUNCTION%%%

%SECTION 1: ACCELERATION
function [v2,t1,P1,a1,l1,timeSection1,preqSection1,poutSection1,velSection1,accelSection1] =
sec1(g,rho,m,csr,crr,v4,cd,A,driveEff,pMotor,tMotor, wheelR, j)

    amax = csr*g;%tMotor/(wheelR*m); %calculates maximum acceleration from the motor torque,
wheel/tire OD, and total mass

    %base values and empty matrices for loop
    t = 0;
    accel = 0;
    time = [];
    acceleration = [];
    velocity = [];
    position = [];
    powerOut = [];
    powerReq = [];

    while accel>=0 %loop creates data for a linear acceleration

        time = [time, t];
        accel=-j*(t)+amax;
        acceleration = [acceleration, accel];
        Vel=-j*((t^2)/2)+(amax*t)+v4;
        velocity = [velocity, Vel];
        Preq=m.*accel.*Vel+ m*g.*Vel.*crr*cos(0)+(1/2)*rho*cd*A.*(Vel).^3;
        powerReq = [powerReq, Preq];
        Pveh_out=Preq/driveEff;
        powerOut = [powerOut, Pveh_out];
        x = ((amax*t^2)/2)-(j*((t^3)/6))+(v4*t);
        position = [position, x];
        t = t + 0.1;

    end

    %remove last data point that goes beyond
    time(:,length(time)) = [];
    acceleration(:,length(acceleration)) = [];
    velocity(:,length(velocity)) = [];
    position(:,length(position)) = [];
    powerOut(:,length(powerOut)) = [];
    powerReq(:,length(powerReq)) = [];

    %max performance values
    t1 = time(end);
    P1 = max(powerOut);
    v2 = max(velocity);
    a1 = acceleration(1);
```

```
    l1 = max(position);

    %output data
    timeSection1 = time;
    preqSection1 = powerReq;%Preq;
    poutSection1 = powerOut;%Pveh_out_effbased;
    velSection1 = velocity;%Vel;
    accelSection1 = acceleration;

end

%SECTION 2: CONSTANT VELOCITY
function [l2,t2,P2, timeSection2, preqSection2, poutSection2, velSection2, accelSection2] =
sec2(v2,L,l1,l3,m,g,crr,cd,A,driveEff)

    %calc cruise distance from straight away lg, accel lg, and decel lg
    l2 = L - l1-l3;
    t2 = l2/v2;

    %calc preq and pout
    P2 = ((m*0*v2)+(m*g*v2*crr)+(.5*1.225*cd*A*(v2^3)));
    P2DE = ((m*0*v2)+(m*g*v2*crr)+(.5*1.225*cd*A*(v2^3)))/(driveEff);

    %creates data
    t=0.1:0.1:t2;
    v = [];
    a = [];
    pReq = [];
    pOut = [];
    i=1;
    while i <= length(t)
        v(i) = v2;
        a(i) = 0;
        pReq(i) = P2;
        pOut(i) = P2DE;
        i = i + 1;
    end

    %outputData
    timeSection2 = t;
    preqSection2 = pReq;
    poutSection2 = pOut;
    velSection2 = v;
    accelSection2 = a;

end

%SECTION 3: DECCELERATION
function [t3,l3,a3, timeSection3, preqSection3, poutSection3, velSection3, accelSection3] =
sec3(j,Vo,Vmax,m,g,crr,rho,A,cd)

    %base values and empty matrices
    t = 0;
    accel = 0;
    time = [];
    acceleration = [];
    velocity = [];
    position = [];
    powerOut = [];
    powerReq = [];
    Vel = 5000;

    %creates data
    while Vel>=Vo %loop creates data for a linear acceleration

        time = [time, t];
        accel=-j*(t);
        acceleration = [acceleration, accel];
```

```
        Vel=-j*((t^2)/2)+Vmax;
        velocity = [velocity, Vel];
        Preq=m*g.*Vel.*crr*cos(0)+(1/2)*rho*cd*A.*(Vel).^3;
        powerReq = [powerReq, Preq];
        Pveh_out=Preq/0.85;
        powerOut = [powerOut, Pveh_out];
        x = -j*((t^3)/6)+Vmax*t;
        position = [position, x];
        t = t + 0.1;

    end

    %remove last data point that goes beyond
    time(:,length(time)) = [];
    acceleration(:,length(acceleration)) = [];
    velocity(:,length(velocity)) = [];
    position(:,length(position)) = [];
    powerOut(:,length(powerOut)) = [];
    powerReq(:,length(powerReq)) = [];

    %output data
    timeSection3 = time;
    preqSection3 = powerReq;
    poutSection3 = powerOut;
    velSection3 = velocity;
    accelSection3 = acceleration;

    %max performance values
    t3 = max(time);
    l3 = max(position);
    a3 = max(acceleration);

end

%SECTION 4: TURN
function [v4, t4, P4DE, l4, timeSection4, preqSection4,poutSection4, velSection4, accelSection4] =
sec4(csr, crr, g, r, m, cd, A, driveEff)

    v4 = sqrt(csr*g*r); %calcs max speed in turn from grip

    %calc lg and time
    l4 = 3.14*r;
    t4 = l4/v4;

    %calcs preq and poutput
    P4 = ((m*0*v4)+(m*g*v4*crr)+(.5*1.225*cd*A*(v4^3)));
    P4DE = ((m*0*v4)+(m*g*v4*crr)+(.5*1.225*cd*A*(v4^3)))/(driveEff);

    %base values and empty matrices
    t=0.1:0.1:t4;
    v = [];
    a = [];
    pReq = [];
    pOut = [];
    i=1;

    %creates data
    while i <= length(t)
        v(i) = v4;
        a(i) = 0;
        pReq(i) = P4;
        pOut(i) = P4DE;
        i = i + 1;
    end

    %output data
    timeSection4 = t;
    preqSection4 = pReq;
```

```
    poutSection4 = pOut;
    velSection4 = v;
    accelSection4 = a;

end
```

APPENDIX D: EXPERIMENTAL TABULATED DATA

Table 2: Data collected from the fuel cell operating between 0.73-8.95 amps without cooling fans and an inlet pressure of 40 psi.

Current (amp)	Voltage (V)	Power (W)
8.95	16.34	146.2
8.82	18.41	162.4
8.74	20.08	175.5
8.63	19.90	171.7
8.52	20.53	174.9
8.42	20.73	174.5
8.32	22.12	184.0
8.22	22.96	188.7
8.13	23.06	187.5
8.03	22.55	181.1
7.03	20.60	144.8
6.02	20.83	125.4
5.02	22.22	111.5
4.03	23.66	95.3
3.02	24.47	73.9
2.02	25.80	52.1
1.03	28.28	29.1
0.93	32.72	30.4
0.81	33.50	27.1
0.73	34.02	24.8

Table 3: Data collected from the fuel cell operating at 1.03 amps with no cooling fans.

Time (s)	**Voltage (V)**	**Temperature (°C)**	**Power (W)**
5	27.80	20.1	28.634
10	28.45	19.9	29.3035
15	29.16	19.9	30.0348
20	29.48	19.9	30.3644
25	29.79	20.2	30.6837
30	29.92	20.6	30.8176
35	30.01	20.9	30.9103
40	30.42	21.4	31.3326
45	30.57	21.9	31.4871
50	30.62	22.3	31.5386
55	30.68	22.7	31.6004
60	30.75	23.1	31.6725
65	30.95	23.6	31.8785
70	31.05	23.9	31.9815
75	31.25	24.3	32.1875
80	31.24	24.7	32.1772
85	31.55	25.0	32.4965
90	31.66	25.4	32.6098
95	31.55	25.8	32.4965
100	31.43	26.2	32.3729
105	31.65	26.6	32.5995
110	31.58	27.0	32.5274
115	31.65	27.2	32.5995
120	31.73	27.4	32.6819
125	31.61	27.6	32.5583
130	31.73	27.7	32.6819
135	31.48	27.8	32.4244
140	31.46	27.9	32.4038
145	31.50	28.1	32.445
150	31.91	28.2	32.8673
155	31.84	28.3	32.7952
160	31.70	28.4	32.651
165	31.78	28.6	32.7334
170	32.03	28.7	32.9909
175	31.91	28.8	32.8673
180	32.03	28.9	32.9909
200	31.83	29.3	32.7849
220	31.77	29.6	32.7231
240	31.73	30.1	32.6819
260	31.59	30.3	32.5377
280	31.51	30.6	32.4553
300	31.31	30.6	32.2493

320	31.23	30.8	32.1669
340	31.13	30.9	32.0639
360	31.05	30.9	31.9815
380	30.88	31.0	31.8064
400	30.90	31.2	31.827
420	30.54	31.3	31.4562
440	30.54	31.4	31.4562
460	30.42	31.6	31.3326
480	30.24	31.6	31.1472

Table 4: Data collected from the fuel cell operating at 1.03 amps with cooling fans operating at 5 V.

Time (s)	**Voltage (V)**	**Temperature (°C)**	**Power (W)**
5	18.47	20.7	19.0241
10	19.86	20.7	20.4558
15	21.60	20.7	22.248
20	23.61	20.8	24.3183
25	25.12	20.9	25.8736
30	25.93	21.1	26.7079
35	26.53	21.3	27.3259
40	27.25	21.5	28.0675
45	27.77	21.7	28.6031
50	28.27	22.1	29.1181
55	28.55	22.3	29.4065
60	28.50	22.6	29.355
65	28.58	22.8	29.4374
70	28.93	22.9	29.7979
75	29.39	23.2	30.2717
80	29.29	23.4	30.1687
85	29.49	23.7	30.3747
90	29.64	23.9	30.5292
95	29.56	24.2	30.4468
100	29.57	24.4	30.4571
105	29.89	24.7	30.7867
110	29.72	24.8	30.6116
115	29.71	25.0	30.6013
120	29.84	25.1	30.7352
125	29.99	25.2	30.8897
130	29.91	25.3	30.8073
135	30.01	25.4	30.9103
140	30.01	25.7	30.9103
145	29.99	25.8	30.8897
150	30.09	26.0	30.9927
155	30.01	25.1	30.9103
160	30.14	26.1	31.0442
165	29.99	26.2	30.8897
170	30.17	26.2	31.0751
175	30.19	26.2	31.0957
180	30.11	26.3	31.0133
200	30.02	26.6	30.9206
220	30.37	26.5	31.2811
240	30.35	26.7	31.2605
260	30.39	26.9	31.3017
280	30.37	27.1	31.2811
300	30.34	27.2	31.2502

320	30.39	27.2	31.3017
340	30.44	27.2	31.3532
360	30.40	27.1	31.312
380	30.25	27.2	31.1575
400	30.25	27.2	31.1575
420	30.29	27.2	31.1987
440	30.11	27.2	31.0133
460	30.34	27.2	31.2502
480	30.25	27.3	31.1575
500	30.14	27.2	31.0442
520	30.19	27.3	31.0957
540	30.32	27.2	31.2296
560	30.12	27.3	31.0236
580	30.19	27.2	31.0957
600	30.11	27.3	31.0133
620	30.17	27.1	31.0751
640	30.01	27.2	30.9103
660	30.07	27.2	30.9721
680	30.17	27.3	31.0751
700	30.11	27.2	31.0133
720	30.07	27.1	30.9721

Table 5: Data collected from the fuel cell operating at 5.02 amps with no cooling fans.

Time (s)	**Voltage (V)**	**Temperature (°C)**	**Power (W)**
5	0.11	21.4	0.55
10	5.44	21.2	27.31
15	11.36	21.1	57.03
20	15.95	21.2	80.07
25	17.18	21.4	86.24
30	18.42	21.8	92.47
35	19.55	22.1	98.14
40	20.54	22.6	103.11
45	21.74	22.9	109.13
50	22.20	23.4	111.44
55	22.74	24.0	114.15
60	23.44	24.4	117.67
65	23.73	24.8	119.12
70	24.46	25.4	122.79
75	24.22	26.1	121.58
80	24.74	26.6	124.19
85	24.77	27.1	124.35
90	24.74	27.5	124.19
95	25.07	27.9	125.85
100	24.47	28.3	122.84
105	25.74	28.7	129.21
110	26.10	29.0	131.02
115	26.00	29.4	130.52
120	26.24	29.9	131.72
125	26.24	30.3	131.72
130	26.34	30.7	132.23
135	26.44	31.0	132.73
140	26.48	31.3	132.93
145	26.48	31.6	132.93
150	26.59	32.0	133.48
155	26.58	32.3	133.43
160	26.64	32.6	133.73
165	26.64	32.9	133.73
170	26.69	33.1	133.98
175	26.76	33.3	134.34
180	26.76	33.5	134.34
200	26.74	34.3	134.23
220	26.69	35.1	133.98
240	26.64	35.6	133.73
260	26.59	36.3	133.48
280	26.49	36.9	132.98
300	26.39	37.3	132.48

320	26.29	37.9	131.98
340	26.19	38.7	131.47
360	26.06	38.7	130.82
380	25.91	39.2	130.07
400	25.78	39.4	129.42
420	25.63	39.7	128.66
440	25.43	39.9	127.66
460	25.27	40.3	126.86
480	25.05	40.6	125.75
500	24.82	41.1	124.60
520	24.45	41.2	122.74
540	24.37	42.1	122.34
560	24.09	42.3	120.93
580	23.86	42.5	119.78
600	23.56	42.9	118.27
620	23.29	43.1	116.92
640	22.93	43.3	115.11
660	22.58	43.7	113.35
680	22.18	44.1	111.34
700	21.69	44.9	108.88
720	21.12	45.2	106.02
740	20.33	45.6	102.06
760	19.19	45.8	96.33
780	17.40	46.1	87.35
800	13.97	46.4	70.13
820	8.73	46.6	43.82
840	0.11	46.9	0.55

Table 6: Data collected from the fuel cell operating at 5.02 amps with cooling fans operating at 5 V.

Time (s)	**Voltage (V)**	**Temperature (°C)**	**Power (W)**
5	20.21	20.8	101.45
10	21.51	20.9	107.98
15	22.63	21.0	113.60
20	23.46	21.1	117.77
25	23.73	21.3	119.12
30	24.24	21.5	121.68
35	24.62	21.9	123.59
40	25.12	22.2	126.10
45	25.28	22.6	126.91
50	25.61	22.9	128.56
55	26.01	23.4	130.57
60	26.05	23.7	130.77
65	26.26	24.1	131.83
70	26.63	24.6	133.68
75	26.72	24.9	134.13
80	26.86	25.4	134.84
85	26.97	25.6	135.39
90	27.07	25.9	135.89
95	27.17	26.2	136.39
100	27.30	26.5	137.05
105	27.45	26.7	137.80
110	27.47	26.9	137.90
115	27.55	27.2	138.30
120	27.60	27.4	138.55
125	27.65	27.6	138.80
130	27.64	27.9	138.75
135	27.72	28.1	139.15
140	27.77	28.2	139.41
145	27.75	28.4	139.31
150	27.77	28.6	139.41
155	27.85	28.7	139.81
160	27.82	28.9	139.66
165	27.92	29.1	140.16
170	27.92	29.2	140.16
175	27.95	29.2	140.31
180	27.92	29.3	140.16
200	28.02	29.8	140.66
220	28.07	30.2	140.91
240	28.10	30.4	141.06
260	28.08	30.6	140.96
280	28.13	30.7	141.21
300	28.13	30.9	141.21

320	28.12	31.1	141.16
340	28.15	31.2	141.31
360	28.15	31.3	141.31
380	28.15	31.3	141.31
400	28.15	31.8	141.31
420	28.15	31.8	141.31
440	28.13	31.9	141.21
460	28.15	32.1	141.31
480	28.13	32.3	141.21
500	28.13	32.4	141.21
520	28.13	32.4	141.21
540	28.13	32.3	141.21
560	28.12	32.3	141.16
580	28.12	32.4	141.16
600	28.12	32.3	141.16
620	28.10	32.6	141.06
640	28.12	32.8	141.16
660	28.10	32.8	141.06
680	28.12	32.7	141.16
700	28.10	32.7	141.06
720	28.10	32.7	141.06
740	28.08	33.0	140.96
760	28.07	32.9	140.91
780	28.07	33.0	140.91
800	28.07	32.9	140.91
820	28.07	32.9	140.91
840	28.05	33.1	140.81
860	28.05	33.0	140.81
880	28.03	33.1	140.71
900	28.05	33.2	140.81
920	28.05	33.2	140.81
940	28.02	33.2	140.66
960	28.03	33.1	140.71
980	28.05	33.1	140.81

Table 7: Data collected from the fuel cell operating at 8.03 amps with no cooling fans.

Time (s)	**Voltage (V)**	**Temperature (°C)**	**Power (W)**
5	0.05	21.3	0.40
10	0.05	21.3	0.40
15	0.06	21.3	0.48
20	0.10	21.4	0.80
25	0.10	21.6	0.80
30	0.15	21.7	1.20
35	1.22	21.9	9.80
40	4.38	22.6	35.17
45	6.76	23.1	54.28
50	8.70	23.9	69.86
55	11.20	24.2	89.94
60	13.72	24.6	110.17
65	14.94	25.2	119.97
70	16.25	25.8	130.49
75	17.03	26.4	136.75
80	17.74	27.1	142.45
85	18.34	27.5	147.27
90	18.80	27.9	150.96
95	19.09	28.5	153.29
100	19.33	29.2	155.22
105	19.52	29.9	156.75
110	19.65	30.3	157.79
115	19.75	30.9	158.59
120	19.78	31.5	158.83
125	19.78	32.1	158.83
130	19.73	32.6	158.43
135	19.65	33.0	157.79
140	19.53	33.6	156.83
145	19.37	34.1	155.54
150	19.20	34.6	154.18
155	19.04	35.0	152.89
160	19.72	35.3	158.35
165	18.44	35.6	148.07
170	18.14	35.9	145.66
175	17.83	36.2	143.17
180	17.41	36.7	139.80
200	15.42	38.1	123.82
220	12.14	39.3	97.48
240	0.18	40.6	1.45

Table 8: Data collected from the fuel cell operating at 8.03 amps with cooling fans operating at 5 V.

Time (s)	**Voltage (V)**	**Temperature (°C)**	**Power (W)**
5	22.68	21.2	182.12
10	23.15	21.2	185.89
15	23.92	21.3	192.08
20	24.07	21.4	193.28
25	24.69	21.6	198.26
30	24.75	21.9	198.74
35	25.18	22.3	202.20
40	25.42	22.7	204.12
45	25.68	23.1	206.21
50	25.96	23.4	208.46
55	26.03	24.0	209.02
60	26.24	24.5	210.71
65	26.34	25.0	211.51
70	26.38	25.6	211.83
75	26.56	26.0	213.28
80	26.59	26.4	213.52
85	26.72	26.9	214.56
90	26.81	27.3	215.28
95	26.82	27.8	215.36
100	26.84	28.2	215.53
105	26.92	28.5	216.17
110	26.91	28.9	216.09
115	26.91	29.1	216.09
120	26.99	29.3	216.73
125	27.01	29.5	216.89
130	27.06	29.7	217.29
135	27.01	29.9	216.89
140	27.11	30.2	217.69
145	27.11	30.6	217.69
150	27.12	30.9	217.77
155	27.16	31.1	218.09
160	27.14	31.3	217.93
165	27.14	31.5	217.93
170	27.17	31.7	218.18
175	27.14	31.9	217.93
180	27.16	32.1	218.09
200	27.21	32.8	218.50
220	27.21	33.5	218.50
240	27.24	33.8	218.74
260	27.22	34.3	218.58
280	27.24	34.7	218.74
300	27.24	35.3	218.74

320	27.21	35.3	218.50
340	27.22	35.2	218.58
360	27.19	35.8	218.34
380	27.19	36.2	218.34
400	27.17	36.1	218.18
420	27.16	36.2	218.09
440	27.16	36.4	218.09
460	27.14	36.8	217.93
480	27.12	37.1	217.77
500	27.11	37.3	217.69
520	27.09	37.5	217.53
540	27.12	37.6	217.77
560	27.12	37.9	217.77
580	27.09	37.5	217.53
600	27.07	37.8	217.37
620	27.06	37.9	217.29
640	27.01	38.3	216.89
660	26.99	38.1	216.73
680	26.97	38.0	216.57
700	26.94	38.3	216.33
720	26.91	38.2	216.09
740	26.87	38.4	215.77
760	26.84	38.2	215.53
780	26.81	38.5	215.28
800	26.77	38.2	214.96
820	26.74	38.5	214.72
840	26.71	39.0	214.48
860	26.68	39.1	214.24
880	26.63	38.9	213.84
900	26.59	38.7	213.52
920	26.56	38.8	213.28
940	26.51	39.2	212.88
960	26.46	39.1	212.47
980	26.41	38.9	212.07
1000	26.38	38.9	211.83
1020	26.33	39.1	211.43
1040	26.29	39.2	211.11
1060	26.24	39.9	210.71
1080	26.23	39.9	210.63
1100	26.14	40.0	209.90
1120	26.11	40.1	209.66
1140	26.06	40.3	209.26
1160	26.01	40.2	208.86
1180	26.00	40.4	208.78
1200	25.90	40.4	207.98

Table 9: Data collected from the fuel cell operating at 8.03 amps with cooling fans operating at 12 V.

Time (s)	**Voltage (V)**	**Temperature (°C)**	**Power (W)**
5	9.13	18.4	73.31
10	12.24	18.4	98.29
15	14.23	18.5	114.27
20	15.92	18.7	127.84
25	17.25	19.1	138.52
30	18.47	19.5	148.31
35	19.42	19.8	155.94
40	20.23	20.2	162.45
45	20.99	20.7	168.55
50	21.65	21.0	173.85
55	22.17	21.2	178.03
60	22.65	21.4	181.88
65	23.10	21.7	185.49
70	23.46	22.0	188.38
75	23.81	22.1	191.19
80	24.11	22.4	193.60
85	24.37	22.7	195.69
90	24.64	22.7	197.86
95	24.82	22.4	199.30
100	25.05	22.2	201.15
105	25.17	22	202.12
110	25.32	21.9	203.32
115	25.48	21.9	204.60
120	25.63	21.9	205.81
125	25.76	21.9	206.85
130	25.90	22.0	207.98
135	25.96	22.0	208.46
140	26.05	22.1	209.18
145	26.16	22.1	210.06
150	26.23	22.1	210.63
155	26.31	22.0	211.27
160	26.34	22.2	211.51
165	26.41	22.3	212.07
170	26.49	22.3	212.71
175	26.53	22.3	213.04
180	26.58	22.4	213.44
200	26.72	22.6	214.56
220	26.82	22.7	215.36
240	26.91	22.8	216.09
260	26.97	22.9	216.57
280	27.01	22.9	216.89
300	27.04	22.5	217.13

320	27.11	22.7	217.69
340	27.12	23.4	217.77
360	27.16	23.7	218.09
380	27.19	23.7	218.34
400	27.21	23.8	218.50
420	27.24	24.1	218.74
440	27.25	24.3	218.82
460	27.27	24.3	218.98
480	27.29	24.3	219.14
500	27.32	24.3	219.38
520	27.32	24.3	219.38
540	27.34	24.3	219.54
560	27.37	24.8	219.78
580	27.39	24.6	219.94
600	27.40	24.6	220.02
620	27.40	24.7	220.02
640	27.44	24.6	220.34
660	27.44	24.8	220.34
680	27.45	24.9	220.42
700	27.45	24.9	220.42
720	27.47	24.9	220.58
740	27.47	24.9	220.58
760	27.49	24.9	220.74
780	27.47	25.1	220.58
800	27.50	24.4	220.83
820	27.50	24.9	220.83
840	27.52	24.9	220.99
860	27.52	24.8	220.99
880	27.54	24.7	221.15
900	27.52	24.7	220.99
920	27.52	24.7	220.99
940	27.54	24.7	221.15
960	27.54	24.7	221.15
980	27.54	24.7	221.15
1000	27.55	24.8	221.23
1020	27.55	24.8	221.23
1040	27.57	24.9	221.39
1060	27.57	24.8	221.39
1080	27.57	25.0	221.39
1100	27.57	24.8	221.39
1120	27.59	24.9	221.55
1140	27.59	24.9	221.55
1160	27.59	25.0	221.55
1180	27.59	24.8	221.55
1200	27.60	24.9	221.63

APPENDIX E: GRAPHS FROM EXPERIMENTAL DATA

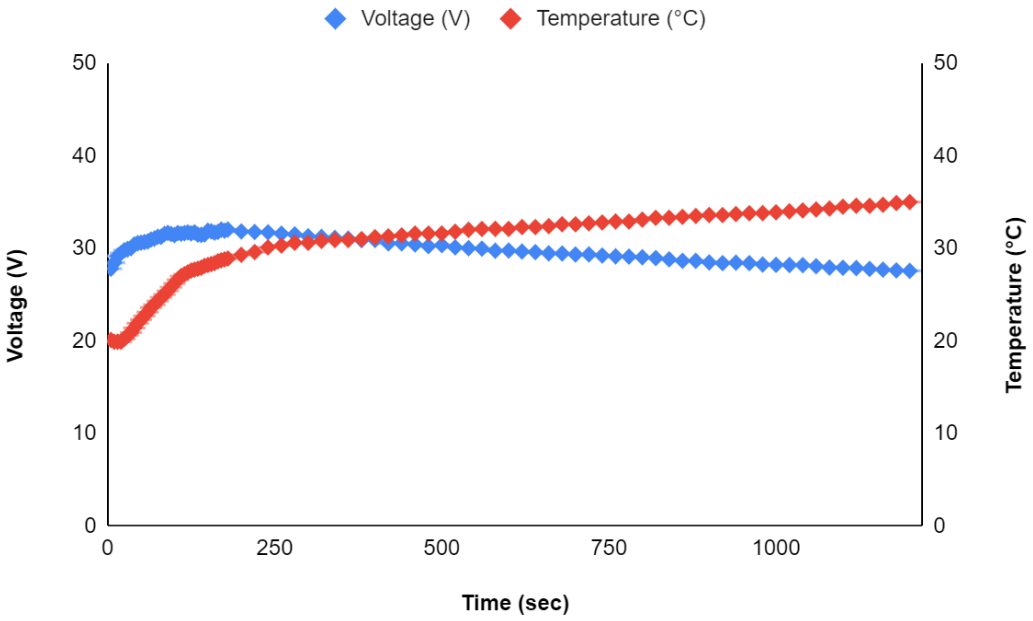

Figure 24: Fuel cell operating at 1.03 amps with no cooling fans.

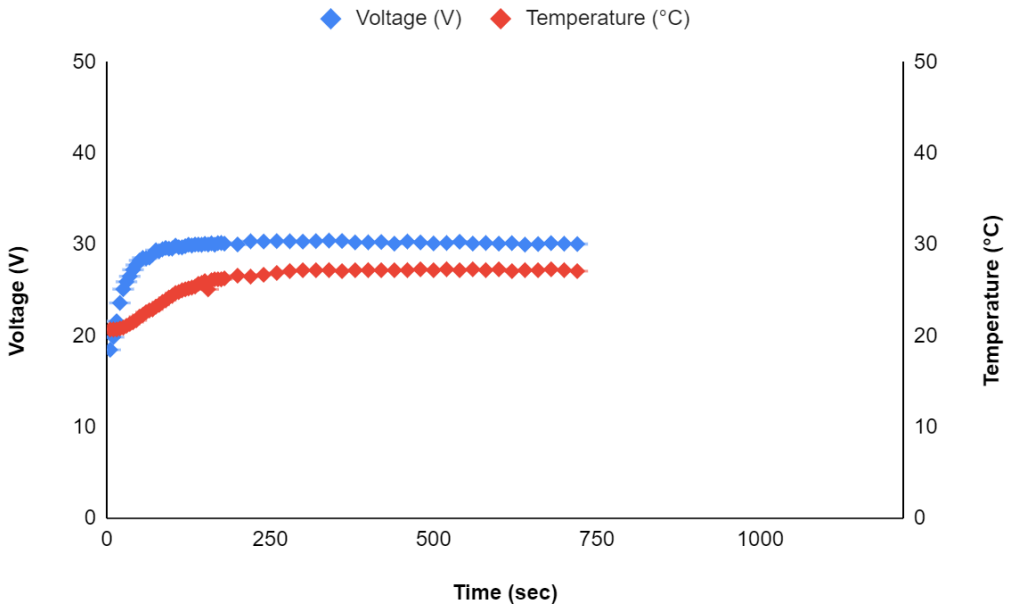

Figure 25: Fuel cell operating at 1.03 amps with cooling fans at 5 V.

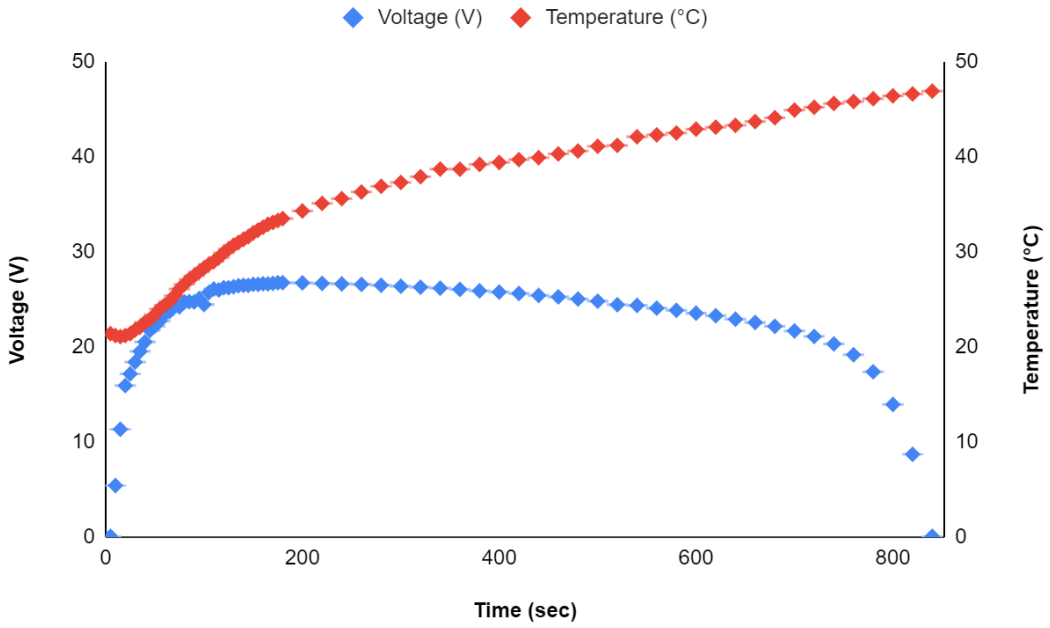

Figure 26: Fuel cell operating at 5.03 amps with no cooling fans.

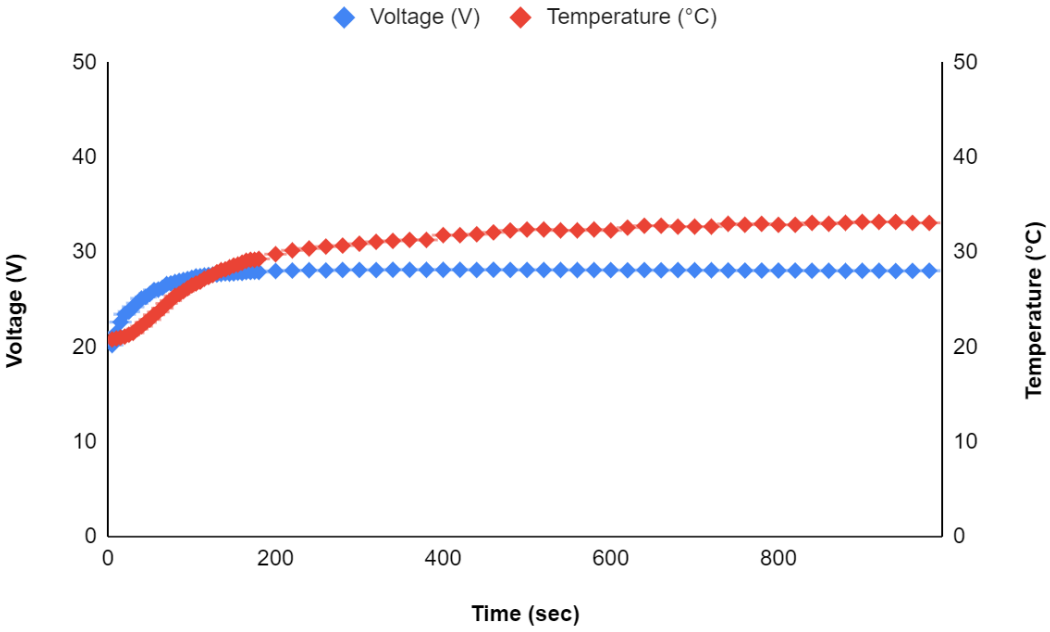

Figure 27: Fuel cell operating at 5.03 amps with cooling fans at 5 V.

APPENDIX F: PHOTOS OF EXPERIMENTAL SET UP

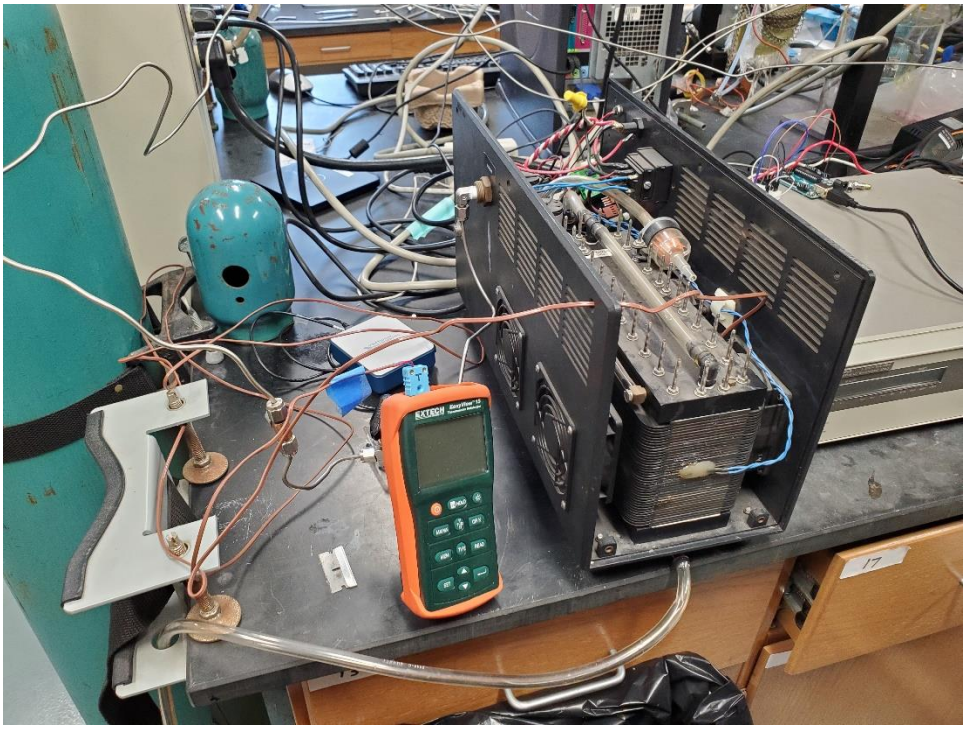

Figure 28: View of fuel cell and thermocouple reader.

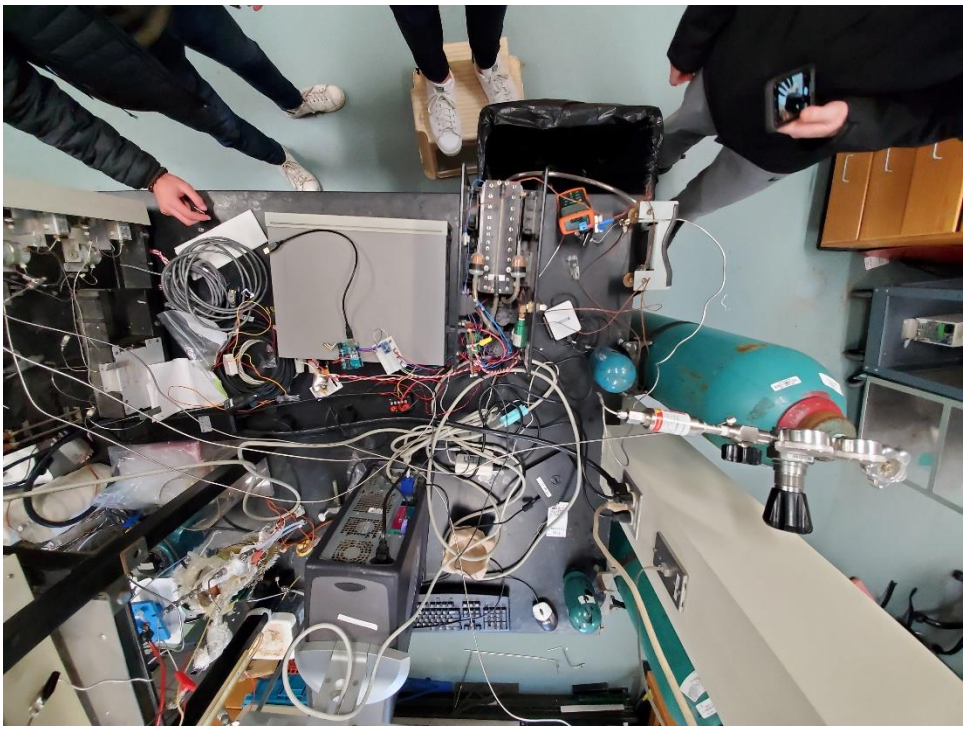

Figure 29: Top view of lab station.

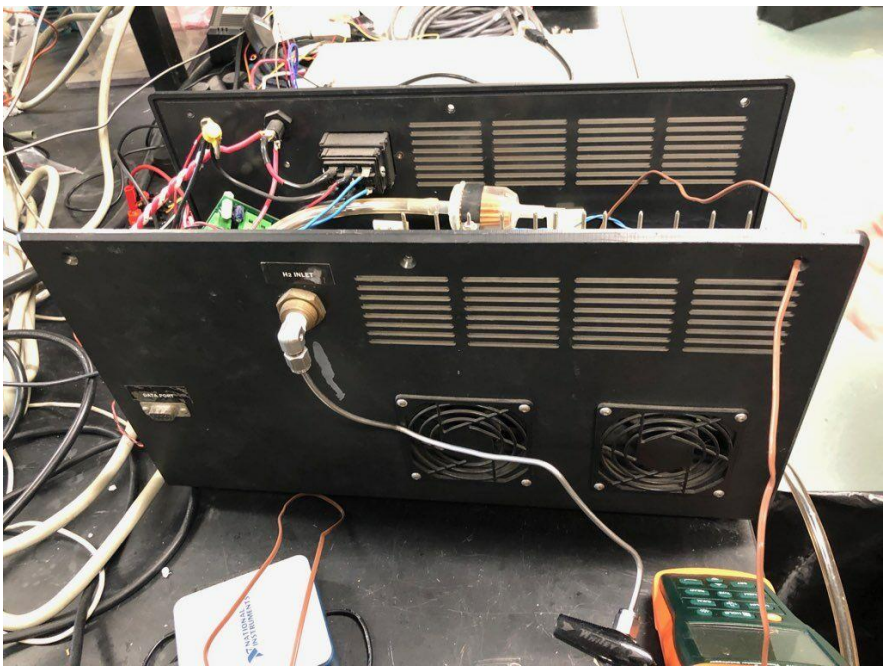

Figure 30: Side view of the PowerPEM-PS250 fuel cell used for experimentation.

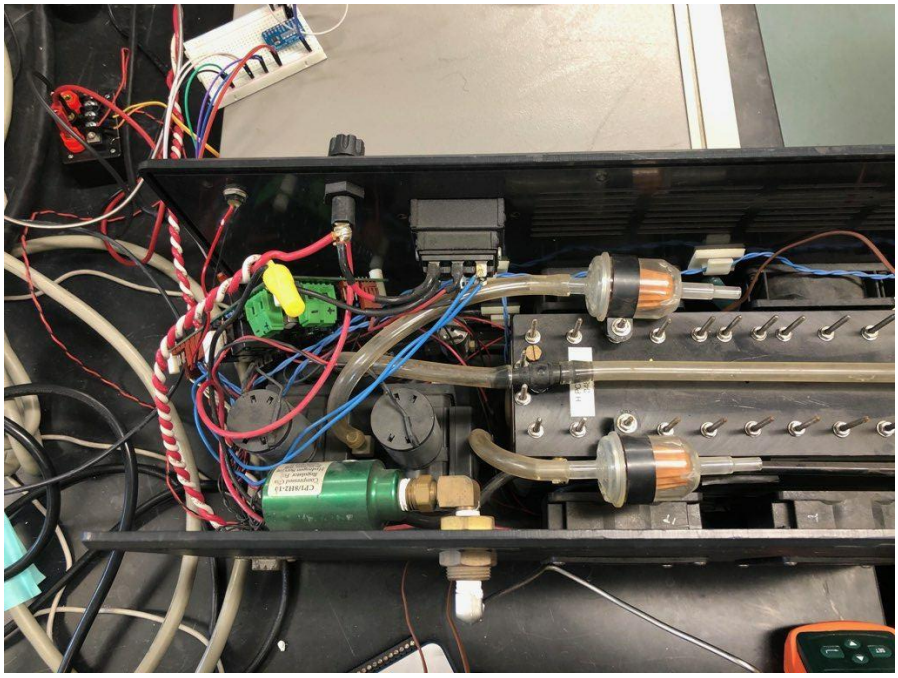

Figure 31: Top view of the PowerPEM-PS250 fuel cell used for experimentation.

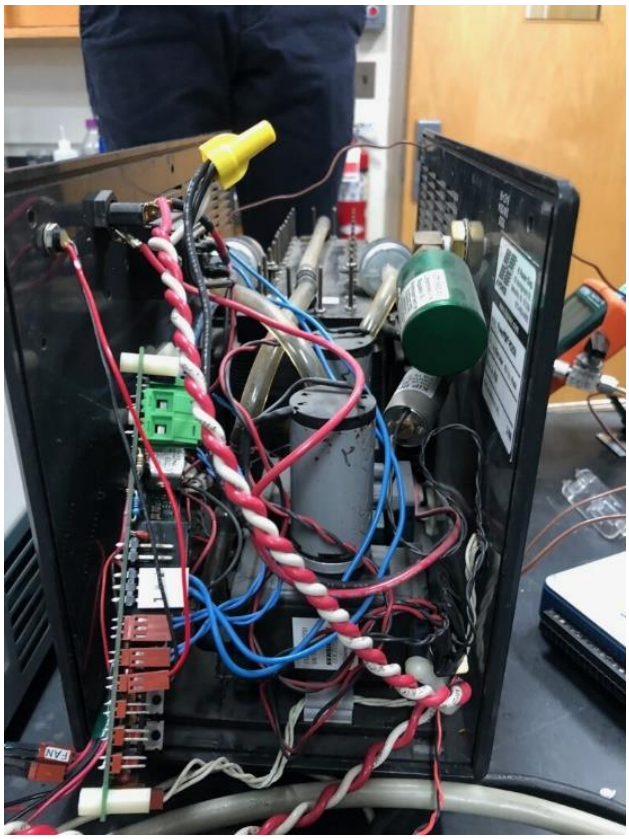

Figure 32: Back view of the PowerPEM-PS250 fuel cell used for experimentation.